

~~CONFIDENTIAL~~

Copy 5 ✓  
RM E57A28

C.2

NACA RM E57A28

**NACA**

# RESEARCH MEMORANDUM

ANALYSIS OF EXPERIMENTAL LOW-SPEED LOSS AND STALL

CHARACTERISTICS OF TWO-DIMENSIONAL

COMPRESSOR BLADE CASCADES

By Seymour Lieblein

Lewis Flight Propulsion Laboratory

CLASSIFICATION CHANGE ~~C~~leveland, Ohio

UNCLASSIFIED **LIBRARY COPY**

*NACA Research  
1 R N-128*

*effectively*  
MAR 25 1957 *June 24, 1958*

By authority of

*AMT 8-12-58*

Date **LANGLEY AERONAUTICAL LABORATORY**  
**LIBRARY, NACA**  
**LANGLEY FIELD, VIRGINIA**

CLASSIFIED DOCUMENT

This material contains information affecting the National Defense of the United States within the meaning of the espionage laws, Title 18, U.S.C., Secs. 793 and 794, the transmission or revelation of which in any manner to an unauthorized person is prohibited by law.

## NATIONAL ADVISORY COMMITTEE FOR AERONAUTICS

WASHINGTON

March 19, 1957

~~CONFIDENTIAL~~

NACA RM E57A28

## NATIONAL ADVISORY COMMITTEE FOR AERONAUTICS

## RESEARCH MEMORANDUM

ANALYSIS OF EXPERIMENTAL LOW-SPEED LOSS AND STALL CHARACTERISTICS  
OF TWO-DIMENSIONAL COMPRESSOR BLADE CASCADES

By Seymour Lieblein

## SUMMARY

CP-1

An analysis of the low-speed experimental loss characteristics of conventional 10-percent-thick low-speed compressor cascade sections is presented in terms of wake momentum thickness and blade velocity diffusion. Blade-wake momentum thickness, expressed as a ratio to the chord length, is computed from various reported loss parameters by means of derived conversion equations. Blade diffusion is expressed as the ratio of measured maximum upper-surface velocity to outlet velocity and as an equivalent ratio expressible in terms of the blade solidity and velocity triangle.

Within the restrictions of the available data, an essentially universal correlation between wake momentum thickness and equivalent diffusion ratio is obtained at angles of attack at minimum loss and greater for a wide range of blade configurations. Further correlations indicate that blade stall at angles of attack at minimum loss and greater, as evidenced by a sharp rise in wake momentum thickness, is possible whenever the equivalent diffusion ratio exceeds a value of about 2. Means of estimating the low-speed total-pressure loss and the unstalled range of operation of conventional cascade sections as functions of solidity, air inlet angle, and air turning angle are obtained, and examples and limitations of the application of the results to blade design are presented.

## INTRODUCTION

Investigations of two-dimensional-cascade sections have frequently been utilized in axial-flow-compressor research to gain an insight into the loss and stall characteristics of compressor blade elements. In particular, it is currently desirable to obtain generalized correlations for cascade losses covering wide ranges of cascade geometries.

In order to facilitate the determination of generalized loss correlations, it is necessary that a loss parameter be used that is independent of the cascade geometry (solidity and chord or air angles) and is a

function of only the individual blade wakes. The theoretical loss analysis of reference 1 shows that the principal wake characteristics that influence the cascade loss are the momentum thickness (expressed nondimensionally as a ratio to the chord length) and the form factor. The wake form factor, however, according to reference 2, is effectively constant at the usual cascade measuring-station location (1 to 1.5 chord lengths downstream of the blade trailing edge) for a wide range of cascade geometries and losses. The primary wake characteristic descriptive of the cascade loss is thus the measuring-station blade-wake momentum thickness. The wake momentum thickness should therefore constitute a fundamental parameter for the correlation of cascade losses.

Since the blade wake is formed from the pressure- and suction-surface boundary layers, the wake momentum thickness will depend on the blade surface velocity distribution. Experience has shown that blade surface velocity distributions that result in large amounts of diffusion in velocity along the surfaces tend to produce relatively thick boundary layers and eventual separation or stall. The concept of velocity diffusion has, therefore, been an important one in the analysis of blade losses. Simplified relations are obtained in references 3 to 8 for the prediction of boundary-layer growth, flow separation, or maximum lift coefficient in terms of surface velocity diffusion.

In the present report, the concept of velocity diffusion is applied in an analysis of blade losses expressed in terms of the fundamental parameter of wake momentum thickness. Wake momentum thicknesses of conventional low-speed cascade blade sections are computed from experimental loss coefficients and correlated against simplified upper (suction) surface diffusion parameters in the range of operation from minimum loss to positive stall. The data correlations are expressed first in terms of measured maximum upper-surface velocities and later, for cases for which surface velocity data are unavailable, in equivalent terms based on inlet and outlet velocities. The question of blade stall is discussed, and considerations are presented for predicting the loss, stall point, and operating range of cascade sections in the range of angle of attack from minimum loss to positive stall. The effects of such factors as blade shape, section thickness, and Reynolds number on the diffusion correlation are also considered.

The analysis is based on the systematic cascade data for the NACA 65-series compressor blade sections of references 9 and 10, and on the limited available data for the British C.4 circular-arc blades of references 11 and 12. Restrictions and limitations involved in the application of the results to cascade performance analyses are discussed.

## SYMBOLS

$A$	aspect ratio, ratio of blade span to mean chord length
$a, b$	constants in loss and diffusion-ratio equations
$C_D$	drag coefficient
$C_{fr}$	wall friction coefficient
$C_{l0}$	isolated lift coefficient (used in designation of NACA 65-series blades)
$C_w$	wake force coefficient
$c$	chord length
$D_{eq}$	equivalent diffusion ratio (defined by eq. (8))
$F$	force
$F_w$	wake momentum force
$H$	wake form factor, $\delta^*/\theta$
$n$	coordinate normal to outlet-flow direction
$P$	total pressure
$\Delta \bar{P}$	averaged decrease in total pressure
$p$	static pressure
$Re_c$	blade-chord Reynolds number
$r$	radius
$s$	blade spacing normal to axial direction
$s_n$	blade spacing normal to outlet flow direction
$t$	blade thickness
$V$	flow velocity
$x$	coordinate along outlet flow direction
$y$	coordinate normal to axial direction

- $z$  coordinate along axial direction  
 $\alpha$  angle of attack, angle between blade chord and inlet-air direction, deg  
 $\beta$  air angle, angle between airflow and axial direction, deg  
 $\Gamma$  circulation parameter  $\frac{\cos^2 \beta_1}{\sigma} (\tan \beta_1 - \tan \beta_2)$   
 $\gamma^0$  blade-chord angle, angle between blade chord and axial direction, deg  
 $\delta$  wake full thickness  
 $\delta^*$  wake displacement thickness  
 $\theta$  wake momentum thickness  
 $\rho$  mass density  
 $\sigma$  solidity, ratio of chord to spacing  
 $\Omega$  total-pressure-loss parameter  $\frac{1}{2} \frac{\bar{\omega}_1}{\sigma} \left( \frac{\cos^3 \beta_2}{\cos^2 \beta_1} \right)$   
 $\bar{\omega}_1$  total-pressure-loss coefficient based on inlet velocity,  $(\Delta \bar{P})_2 / \frac{1}{2} \rho V_1^2$   
 $\bar{\omega}_2$  total-pressure-loss coefficient based on outlet velocity,  $(\Delta \bar{P})_2 / \frac{1}{2} \rho V_{0,2}^2$   
 $\bar{\omega}_{1,\infty}$  total-pressure-loss coefficient for complete mixing based on inlet velocity,  $(\Delta \bar{P})_\infty / \frac{1}{2} \rho V_1^2$   
 $\bar{\omega}_{2,\infty}$  total-pressure-loss coefficient for complete mixing based on outlet velocity,  $(\Delta \bar{P})_\infty / \frac{1}{2} \rho V_{0,2}^2$

## Subscripts:

- $A$  area average  
 $D$  drag

4222

L lift  
l lower surface  
M mass average  
m vector mean condition  
max maximum  
n normal to outlet flow direction  
ref reference  
s stall  
te plane of trailing edge  
u upper surface  
y normal to axial direction  
z axial direction  
0 free stream  
1 inlet  
2 outlet measuring station  
∞ far downstream where complete mixing has taken place

Superscript:

\* reference minimum-loss value

#### DATA SOURCES

The cascade loss data used in the analysis were obtained from investigations of the NACA 65-(A<sub>10</sub>)-series blades in reference 9, the NACA 65-(AI)-series blades in reference 10, and the British C.4 circular-arc mean-line blades in references 11 and 12. All blades are low-speed thick-nose profiles of 10-percent maximum thickness. Both the NACA 65-(C<sub>10</sub>A<sub>10</sub>)10 blades (ref. 9) and the circular-arc blades (refs. 11 and 12), whose mean camber lines are symmetrical about the midchord point,

4222

tend to give uniform chordwise design pressure loading. The NACA 65-(C<sub>10</sub>A<sub>2</sub>I<sub>8b</sub>)10 blade of reference 10 is a rearward loading section; the 65-(C<sub>10</sub>A<sub>6</sub>I<sub>4</sub>)10 blade (ref. 10) is a forward loading section; and the 65-(C<sub>10</sub>A<sub>6</sub>I<sub>4b</sub>)10 blade (ref. 10) is partway between the A<sub>10</sub> and A<sub>2</sub>I<sub>8b</sub> mean lines. The various blade shapes considered are described and compared in references 10 and 12.

Identification information concerning the various blade configurations and cascade tunnels used in the data sources is given in table I. In all cases, because of the tunnel size, boundary-layer control, or operating techniques employed, good two-dimensionality was obtained in the cascade flow. Blade-chord Reynolds numbers were between about  $2.0 \times 10^5$  and  $4.5 \times 10^5$ .

### CALCULATIONS

As indicated previously, the data correlations are to be expressed in terms of the fundamental loss parameter of wake momentum thickness. Because of the general absence of specific experimental data describing the characteristics of the wakes of cascade blades, it was necessary to establish methods for computing the nondimensional wake momentum thickness from the particular loss parameters used in the various cascade investigations. The principal loss parameters in use in cascade research are the wake coefficient  $C_w$  (ref. 9), the drag coefficient  $C_D$  (refs. 9 and 11), and the total-pressure-loss coefficient  $\bar{w}_1$  (ref. 4). The various equations and techniques obtained for computing the nondimensional momentum thickness at the cascade measuring station  $(\theta/c)_2$  from these loss parameters are developed in appendixes A to E. The developments assume incompressible flow and an outlet flow model as shown in figures 1 and 2. True two-dimensional flow is assumed for all the data converted. The calculation of  $(\theta/c)_2$  for a given magnitude of loss parameter, as indicated in the appendixes, requires a knowledge of the air inlet and outlet angles, the cascade solidity, and the wake form factor.

For the NACA 65-series blades of references 9 and 10, wake momentum thickness  $(\theta/c)_2$  was computed from the measured wake coefficient according to equation (A12) in appendix A. For the C.4 blades of references 11 and 12,  $(\theta/c)_2$  was computed from the measured drag coefficients according to equations (B16) and (B18), respectively. Total-pressure-loss coefficient  $\bar{w}_1$  was computed for simplicity in all cases from the measured drag coefficients according to equation (E1) or (E2).

An example of the variations of computed  $(\theta/c)_2$  and  $\bar{w}_1$  with angle of attack is given in figure 3. Figure 3 also shows the definition of the

reference point of minimum loss. From plots such as figure 3, the variations of  $(\theta/c)_2$  with the pertinent correlation parameters considered were then obtained.

In many cases, erratic variations of loss parameter were observed in the original data because of sudden changes in the boundary-layer flow arising from local laminar separations. An illustrative plot of the variation of computed momentum thickness with angle of attack for a cascade with local laminar separation is shown in figure 4. In such instances, it was necessary to estimate the probable variation of the loss parameter in the absence of a local laminar separation (as indicated in the figure) and use values obtained from the faired curves for the correlations. Erratic loss curves were observed for the 65-(C<sub>70</sub>A<sub>10</sub>)10 blades of reference 9, the 65-(C<sub>70</sub>A<sub>2</sub>I<sub>8b</sub>)10 blades of reference 10, and the blades of reference 11. The 65-(12A<sub>6</sub>I<sub>4</sub>)10 and 65-(12A<sub>6</sub>I<sub>4b</sub>)10 blades of reference 10 and the circular-arc blade of reference 12 were comparatively free of erratic boundary-layer changes.

Because of the factors involved in the calculation procedure, certain unavoidable errors may be introduced in the determination of  $(\theta/c)_2$  as a result of inconsistencies and inaccuracies in either the original loss-parameter determination or in the subsequent conversion to wake momentum thickness, or both. However, it is believed that any errors involved in the calculation of  $(\theta/c)_2$  will be small enough not to mask the principal results of the final correlations.

## ANALYSIS

### Approach

Examination of blade surface velocity distributions of conventional cascade sections, as illustrated in figure 5, shows that, for angles of attack greater than those at about the point of reference minimum loss (as defined in fig. 3), large negative gradients of velocity exist on the upper (suction) surface of the blade. In this region of blade operation, the upper-surface boundary layer contributes the major share of the wake, and, therefore, the upper-surface velocity distribution becomes the governing factor in the determination of the wake loss. The general hypothesis of the diffusion approach considers that, in the range of blade operation from minimum loss to positive stall, the momentum thickness of the blade wake varies with the diffusion in velocity on the upper surface of the blade. It is further considered that, for conventional velocity distributions as illustrated by figure 5, the diffusion in velocity can be expressed significantly as a parameter involving the maximum surface velocity and the outlet velocity. In the present analysis, the velocity diffusion is expressed in terms of the ratio of the maximum upper-surface



velocity to the outlet free-stream velocity  $V_{\max}/V_{0,2}$ . The first part of the analysis, therefore, presents a correlation of wake momentum thickness with blade surface diffusion ratio  $V_{\max}/V_{0,2}$  to determine the validity of the diffusion assumption. Correlations are presented for the reference minimum-loss point and for greater angles of attack.

Since blade surface velocity distribution data are not generally available for all usable blade shapes, it is desirable to investigate ways of extending the diffusion correlation to cases for which the surface velocity characteristics are unknown. To accomplish this, appropriate empirical relations were investigated between the surface diffusion ratio  $V_{\max}/V_{0,2}$  and derived readily calculated quantities based only on inlet and outlet flow conditions. Equivalent diffusion ratios based on over-all velocities are then established from these empirical relations.

#### Blade Surface Diffusion Ratio

The initial correlation of wake momentum thickness against suction-surface diffusion ratio  $V_{\max}/V_{0,2}$  was made for the reference condition of minimum-loss angle of attack as defined in figure 3. For simplicity, the free-stream outlet velocity  $V_{0,2}$  was computed from measured air angles such that<sup>1</sup>

$$\frac{V_{\max}}{V_{0,2}} = \frac{V_{\max}}{V_1} \frac{V_1}{V_{0,2}} = \frac{V_{\max}}{V_1} \frac{\cos \beta_2}{\cos \beta_1} \quad (1)$$

where  $V_{\max}/V_1$  was determined from the plots of experimental upper-surface velocity distribution in the data references. Values of  $(\theta/c)_2$  and  $V_{\max}/V_{0,2}$  at minimum loss for a given blade section were obtained from faired curves of these quantities against angle of attack (as illustrated in fig. 3 for  $(\theta/c)_2$ ).

Correlation at minimum-loss angle of attack. - The plot of  $(\theta/c)_2$  against  $V_{\max}/V_{0,2}$  at reference minimum-loss angle of attack obtained from the available cascade data covering a wide range of cambers, solidities, and air inlet angles is shown in figure 6. The data are plotted in

<sup>1</sup>Theoretically, in two-dimensional-cascade flow with wakes, the ratio of approximate  $V_{0,2}$  (as determined from only the cosines of the air angles, eq. (1)) to exact  $V_{0,2}$  is given by the following (from eq. (A10)):

$$\frac{(V_{0,2})_{\text{approx}}}{(V_{0,2})_{\text{exact}}} = 1 - \left(\frac{\theta}{c}\right)_2 \frac{\sigma H_2}{\cos \beta_2} \quad (2)$$

two parts: because of their similar surface velocity distributions and blade-chord Reynolds numbers, the 65-(A<sub>10</sub>)-series blades (ref. 9) and the C.4 circular-arc blades (refs. 11 and 12) are presented together in figure 6(a); and the 65-(AI)-series blades of reference 10 are plotted in figure 6(b).

Figure 6(a) provides an essential confirmation of the basic diffusion hypothesis for the 65-(C<sub>70</sub>A<sub>10</sub>)10 blade, in that a well-defined correlation is obtained between  $(\theta/c)_2$  and  $V_{\max}/V_{0,2}$  for a wide range of blade configurations. It also appears, from the limited available data (solid symbols in fig. 6(a)), that the C.4 circular-arc blades should exhibit a similar correlation.

For a velocity ratio of 1 (no diffusion), the data of figure 6(a) extrapolate to a value of  $(\theta/c)_2$  of about 0.004. For the hypothetical condition of  $V_{\max}/V_{0,2}$  equal to 1, the blade surface flow should correspond essentially to flat-plate flow. For the flat plate at a Reynolds number of  $2.5 \times 10^5$ , the wake momentum thickness for two surfaces is obtained from the wall friction coefficient ( $\theta/c = C_{fr}/2$  for a surface) as 0.0027 for completely laminar flow and 0.0059 for completely turbulent flow (ref. 13, fig. 88, e.g.). It is expected, therefore, that the extrapolated value of  $(\theta/c)_2$  at  $V_{\max}/V_{0,2} = 1$  in figure 6(a) would lie between these two values.

On the high-diffusion-ratio end of the plot in figure 6(a), there are two points at a  $V_{\max}/V_{0,2}$  of about 2.1 that appear to fall somewhat above the indicated band of the correlation. Whether these high points are the result of experimental error or reflect some significant increase in the spread of the data at high diffusion ratios is not apparent from these data.

Figure 6(b) indicates that, with minor exceptions, the data from the 65-(AI)-series blades of reference 10 fall within the limits of the data for the 65-(A<sub>10</sub>)-series blades and the C.4 circular-arc blades (dashed curves in fig. 6(b)). The two high values of  $(\theta/c)_2^*$  between  $(V_{\max}/V_{0,2})^*$  of 1.50 and 1.55 for the 65-(C<sub>70</sub>A<sub>2</sub>I<sub>8b</sub>)10 blade are not considered to indicate any significant departures from the principal correlation of figure 6(a). It is believed that these high points are the result of extensive laminar separation effects that could not be faired out in the plots of  $(\theta/c)_2$  against  $\alpha$ .

The two low points for the 65-(12A<sub>6</sub>I<sub>4</sub>)10 blade in figure 6(b), however, are believed to be due to a fundamental effect. It is noted in figure 5 that the blade (fig. 5(d)) has a considerably smaller velocity deceleration on the lower surface at minimum-loss angle of attack than

all the other blades. A smaller lower-surface boundary layer and, consequently, a smaller wake momentum thickness should therefore result for the same values of upper-surface diffusion for this blade.

Correlation over range of angle of attack. - A further indication of the momentum-thickness variations at high diffusion ratios is obtained from the plot of  $(\theta/c)_2$  against  $V_{\max}/V_{0,2}$  for all data points at angles of attack greater than the minimum-loss point ( $\alpha > \alpha^*$ ), as shown in figure 7. As for the case of figure 6, values of  $(\theta/c)_2$  appearing in the plots are faired values. Furthermore, data points for which the measured  $V_{\max}/V_1$  ratios appeared to be unreasonable, like the high  $\alpha$  points for  $C_{l0}$  of 1.2 in figure 11, are omitted in the correlation.

For the 65-( $C_{l0}A_{l0}$ )10 blades in figure 7(a), in general, a correlation similar to that at minimum loss (fig. 6(a)) is obtained, but a wide dispersion of the data occurs for  $V_{\max}/V_{0,2}$  greater than about 2. It could not be determined, because of insufficient data, whether the C.4 circular-arc blade shows a similar characteristic at high diffusion ratios. (Velocity-distribution data at high angles of attack were not available for blade 2.)

Some of the scatter of the data at  $V_{\max}/V_{0,2} > 2$  in figure 7(a) may be attributed to the use of the approximate  $V_{0,2}$  for the diffusion ratio, since the error involved tends to increase with increasing  $(\theta/c)_2$  (see eq. (2)). However, such effects were not sufficient to account for the wide spread of the data. Another factor influencing the data spread may be differences in the reduction in blade circulation arising from the growth of the upper-surface boundary layer for the different cascade geometries. This effect would tend to give different values of measured  $V_{0,2}$  for a given wake momentum thickness.

Furthermore, there are undoubtedly specific differences in the individual developments of the blade surface boundary layers that contribute to the spread of the data in the high-loss region. It was thought that large differences in boundary-layer developments might arise from the extremely steep velocity gradients that occur on the upper surface at the leading edge for many of the blades at high angles of attack. However, such an effect was not distinguishable from the loss and velocity-distribution data available. If separation of the upper-surface boundary layer occurs in this region (as is strongly suspected), there may be large differences in the terminal values of  $(\theta/c)_2$ , depending on whether a complete breakaway or gradual thickening of the boundary layer ensues. There is also the possibility that local laminar separation effects may yet be present at these high angles of attack. Finally, in view of the large velocity gradients existing in the leading-edge region and the finite spacing between pressure taps, the recorded peak velocities may not necessarily be the true maximum values.

At any rate, it is obvious that the correlation between  $(\theta/c)_2$  and  $V_{\max}/V_{0,2}$  in figure 7(a) breaks down for values of diffusion ratio greater than about 2 for the 65-(C<sub>70</sub>A<sub>10</sub>)10 blades. It is also reasonable to interpret the high data points at minimum loss in figure 6(a) as indicating the same type of wide  $(\theta/c)_2$  spread at high  $V_{\max}/V_{0,2}$  as in figure 7(a). Thus, the correlations of figures 6(a) and 7(a) show that a value of suction-surface  $V_{\max}/V_{0,2}$  of about 2 delineates the region of diffusion ratio above which large increases in momentum thickness are possible for angles of attack at minimum loss and greater for the 65-(C<sub>70</sub>A<sub>10</sub>)10 blades.<sup>2</sup>

In the range of diffusion ratio less than 2, somewhat smaller values of  $(\theta/c)_2$  are obtained for  $\alpha > \alpha^*$  in figure 7(a) than at  $\alpha^*$  (fig. 6(a)). This difference is believed due mainly to the more favorable pressure-surface velocity distribution, and therefore smaller pressure-surface wake contribution, at high angles of attack (see fig. 5).

For the 65-(AI)-series blades of reference 10, a somewhat different picture is obtained, as indicated in figure 7(b). For the 65-(12A<sub>6</sub>I<sub>4</sub>)10 and 65-(12A<sub>6</sub>I<sub>4b</sub>)10 blades and for most of the 65-(C<sub>70</sub>A<sub>2</sub>I<sub>8b</sub>)10 blades, the  $(\theta/c)_2$  data fall within the limits of the data for the 65-(C<sub>70</sub>A<sub>10</sub>)10 blades in figure 7(a) (as indicated by the dashed lines in fig. 7(b)). However, there are many points that fall far above the upper limit. Most of the high points below  $V_{\max}/V_{0,2}$  of 1.8 belong to the blades that produced the two high points in figure 6(b). These discrepancies can be attributed to local laminar separation effects.

There may also be some question about the significance of the high points at  $V_{\max}/V_{0,2}$  greater than 1.8. (These values are all high-angle-of-attack points for the high-cambered blades at  $\beta_1$  of 45° and 60°.) At high angles of attack, the 65-(C<sub>70</sub>A<sub>2</sub>I<sub>8b</sub>)10 blades experienced severe localized gradients of velocity on the upper surface at the leading edge (see ref. 10 and fig. 5(e)). It is quite possible that the true maximum values of velocity may fall between the surface pressure taps and be substantially greater than the maximum values recorded at the tap (the values of  $V_{\max}$  used in the plot of fig. 7(b) are maximum tap readings). However, if the recorded values are true maximums, then these blades at their particular test conditions represent a limitation of the validity of the diffusion hypothesis in terms of  $V_{\max}/V_{0,2}$ .

<sup>2</sup>With  $(\theta/c)_2 < 0.02$  for  $V_{\max}/V_{0,2} \leq 2.0$ , from equation (2), the approximate  $V_{0,2}$  used in the diffusion ratio can be up to about 10 percent less than the exact value in a true two-dimensional flow for  $\beta_2$  of 70° and  $\sigma$  of 1.5. The limiting diffusion ratio based on an exact  $V_{0,2}$  may then be as low as 1.8.

### Equivalent Diffusion Ratio

In order to extend the diffusion correlation to design and analysis cases for which surface velocity data are unavailable, it is desirable to establish an equivalent diffusion ratio approximately equal to  $V_{\max}/V_{0,2}$  that is based on readily calculated inlet and outlet conditions. The determination of an equivalent diffusion ratio is based on equation (1). With  $V_1/V_{0,2}$  obtained as before from  $\cos \beta_2/\cos \beta_1$ , it remains to establish an empirical correlation for  $V_{\max}/V_1$ .

In general, the maximum upper-surface velocity ratio  $V_{\max}/V_1$  in the leading-edge region of a conventional blade section is determined by the effects of the blade thickness, the blade circulation, and the angle of attack (ref. 14). Examination of available cascade data shows that  $V_{\max}/V_1$  can be correlated against the product of the ratio of blade circulation to inlet velocity and the cosine of the air inlet angle. This product, called the circulation parameter  $\Gamma$ , in incompressible two-dimensional flow is given by

$$\Gamma = \frac{\cos^2 \beta_1}{\sigma} (\tan \beta_1 - \tan \beta_2) \quad (3)$$

The correlation for  $V_{\max}/V_1$  against circulation parameter for the data at minimum-loss angle of attack is shown in figure 8. An empirical equation for  $V_{\max}/V_1$  at minimum loss is readily derived for the 65-(C<sub>10</sub>A<sub>10</sub>)10 and C.4 circular-arc blades, as shown in figure 8(a), to be

$$\frac{V_{\max}}{V_1} = 1.12 + 0.61 \frac{\cos^2 \beta_1}{\sigma} (\tan \beta_1 - \tan \beta_2) \quad (4)$$

The empirical variation of equation (4) is not as effectively representative of the 65-(AI)-series blades as revealed in figure 8(b). However, as will be shown later, this is of no serious consequence. The equivalent diffusion ratio at minimum loss designated by the symbol  $D_{eq}^*$  is then obtained in terms of inlet and outlet conditions from equations (1) and (4) as

$$D_{eq}^* = \frac{\cos \beta_2}{\cos \beta_1} \left[ 1.12 + 0.61 \frac{\cos^2 \beta_1}{\sigma} (\tan \beta_1 - \tan \beta_2) \right] \left( \frac{V_{\max}}{V_{0,2}} \right)^* \quad (5)$$

The corresponding plot of  $(\theta/c)_2^*$  against  $D_{eq}^*$  at minimum loss is shown in figure 9. For the 65-(C<sub>10</sub>A<sub>10</sub>)10 blades in figure 9(a), although the band of the data is somewhat greater in figure 9(a) than in figure 6(a), the average values and rates of increase of  $(\theta/c)_2^*$  are considered

to be satisfactorily expressed in terms of the equivalent diffusion ratio of equation (5). It is also noted in figure 9(b) that good correlation is obtained for all of the 65-(AI)-series blades. The 65-(12A<sub>6</sub>I<sub>4</sub>)10 blades (blade 6), which had previously appeared low in the plots against  $V_{\max}/V_{0,2}$  (fig. 6(b)), now fall in line with the other data, because the computed values of  $D_{eq}^*$  are smaller than the measured values of  $(V_{\max}/V_{0,2})^*$ . The lower values of  $D_{eq}^*$  obtained for these blades are due to the smaller values of  $(V_{\max}/V_1)^*$  given by the empirical variation of equation (4) (fig. 8(b)).

For angles of attack greater than minimum-loss angle of attack  $\alpha^*$ , the correlation between  $V_{\max}/V_1$  and the circulation parameter  $\Gamma$  varies with the magnitude of the angle difference  $\alpha - \alpha^*$ . As shown by the illustrative plot in figure 10, the slope of the variation tends to remain fixed but the intercept value changes with  $\alpha - \alpha^*$ . Although considerable scatter existed in the original data, especially at large values of  $\alpha - \alpha^*$ , it was possible to derive an average empirical relation for the increase in  $V_{\max}/V_1$  due to increasing angle of attack in the form

$$\Delta\left(\frac{V_{\max}}{V_1}\right) = a(\alpha - \alpha^*)^b \quad (6)$$

From the data for the 65-(C<sub>70</sub>A<sub>10</sub>)10 blades, it was found that  $a = 0.0117$  and  $b = 1.43$ . These constants also satisfactorily described the variations of  $V_{\max}/V_1$  with  $\alpha - \alpha^*$  for the 65-(AI)-series blades, except that the predicted values are somewhat higher than the measured values for the high-cambered 65-(C<sub>70</sub>A<sub>2</sub>I<sub>8b</sub>)10 blade. However, since some question exists concerning the validity of the observed values of  $V_{\max}/V_1$  for these blades (see p. 11), it was decided to use the same constants for all blades with the 65-010 basic thickness distribution. From the very limited available data for the 10-percent-thick British C.4 circular-arc blade, it appears that the effect of increase in angle of attack on  $V_{\max}/V_1$  may be somewhat less than for the 65-series blades, with  $a = 0.007$  and  $b$  remaining as before.

It is thus established that

$$\frac{V_{\max}}{V_1} = 1.12 + a(\alpha - \alpha^*)^{1.43} + 0.61 \frac{\cos^2 \beta_1}{\sigma} (\tan \beta_1 - \tan \beta_2) \quad (7)$$

An example of the comparison between measured and derived values of  $V_{\max}/V_1$  for the 65-(C<sub>70</sub>A<sub>10</sub>)10 blades of reference 9 is given in figure 11. From equations (1) and (7), then, the equivalent diffusion ratio becomes

$$D_{eq} = \frac{\cos \beta_2}{\cos \beta_1} \left[ 1.12 + a(\alpha - \alpha^*)^{1.43} + 0.61 \frac{\cos^2 \beta_1}{\sigma} (\tan \beta_1 - \tan \beta_2) \right] \quad (8)$$

where  $a = 0.0117$  for the 65-series blade, and  $a = 0.007$  for the C.4 circular-arc blade.

According to equation (8), the equivalent diffusion ratio of a blade section at any angle  $(\alpha - \alpha^*)$  can be determined, for a given solidity and air inlet angle, if the air outlet angle  $\beta_2$  is known. It is proposed that  $\beta_2$  be determined in the following manner. If it is assumed that the air turning angle  $(\Delta\beta = \beta_1 - \beta_2)$  varies essentially linearly with angle of attack in the region from minimum loss to positive stall, then

$$\beta_2 = \beta_1 - \Delta\beta = \beta_1 - \Delta\beta^* - \frac{d(\Delta\beta^*)}{d\alpha} (\alpha - \alpha^*) \quad (9)$$

where  $\Delta\beta^*$  is the turning angle and  $d(\Delta\beta^*)/d\alpha$  is the slope of the turning-angle variation at minimum loss. Representative values of  $d(\Delta\beta^*)/d\alpha$  as a function of  $\sigma$  and  $\beta_1$  derived from examination of available cascade data are given in figure 12, and values of minimum-loss  $\alpha^*$  and  $\Delta\beta^*$  are listed in table II. Values of  $\Delta\beta^*$  and  $\alpha^*$  for other cambers, solidities, or air inlet angles can be determined from the available turning-angle rules for the particular blade shape (e.g., Carter's rule of ref. 15 for the circular-arc blade).

Plots of  $(\theta/c)_2$  against equivalent diffusion ratio  $D_{eq}$  given by equation (8) in conjunction with equation (9) for measured data points at angles of attack greater than minimum loss are shown in figure 13 for all blades. (More points are available for the plots of  $(\theta/c)_2$  against  $D_{eq}$  than against measured surface  $V_{max}/V_{0,2}$ , since velocity-distribution data were taken at only a few of the test angles of attack.) For the 65-(A<sub>10</sub>)10 blades (fig. 13(a)), although a somewhat greater scatter of the data exists than in the original plot in terms of  $V_{max}/V_{0,2}$  in figure 7(a) (primarily because of the scatter in the  $V_{max}/V_1$  correlation), a value of  $D_{eq}$  of about 2, as before, delineates the region of possible rapid rise in loss. A similar situation is observed in the corresponding plot for the C.4 circular-arc blades shown in figure 13(b). (A value of  $a = 0.007$  was used in the calculation of diffusion ratio for these blades.)

For the 65-(C<sub>10</sub>A<sub>2</sub>I<sub>8b</sub>)10 blades (fig. 13(c)), it is now found that just about all the data fall within the limits of the 65-(C<sub>10</sub>A<sub>10</sub>)10 blades. The improved correlation is the result of greater computed magnitudes of  $D_{eq}$  compared with the original values of  $V_{max}/V_{0,2}$  for the

high data points in figure 7(b). The higher values of  $D_{eq}$  are a reflection primarily of the higher computed values of  $V_{max}/V_1$ , as mentioned previously. The data for the 65-(12A<sub>6</sub>I<sub>4b</sub>)10 and 65-(12A<sub>6</sub>I<sub>4</sub>)10 blades also fall within the limits of the previous correlations, as indicated in figure 13(d).

### Loss Parameter

As indicated previously, cascade loss data have been presented in terms of various parameters. If the determination or calculation of the more fundamental wake momentum thickness  $(\theta/c)_2$  is not feasible, a significant substitute loss parameter in terms of the total-pressure-loss coefficient  $\bar{w}_1$  can be established for use in cascade loss analyses.

Theoretically, for incompressible two-dimensional-cascade flow, from equation (C7) of appendix C, the wake momentum thickness is given by

$$\left(\frac{\theta}{c}\right)_2 = \frac{\bar{w}_1}{2\sigma} \frac{\cos^3 \beta_2}{\cos^2 \beta_1} \left\{ \frac{3H_2 - 1}{2H_2} \left[ 1 - \left(\frac{\theta}{c}\right)_2 \frac{H_2 \sigma}{\cos \beta_2} \right]^3 \right\} \quad (10)$$

At conventional cascade measuring-station locations (1 to 1.5 chord lengths downstream),  $H_2$  varies little with blade configuration or angle of attack, being of the order of 1.08 (appendix D). Thus, for the values of  $(\theta/c)_2$  obtained over most of the diffusion range, the variation of the terms within the braces will be comparatively small. The wake momentum thickness will therefore vary primarily with the terms preceding the braces. A substitute loss parameter  $\Omega$  reflecting the momentum thickness  $(\theta/c)_2$  can thus be established as

$$\Omega = \frac{1}{2} \frac{\bar{w}_1}{\sigma} \frac{\cos^3 \beta_2}{\cos^2 \beta_1} \quad (11)$$

A plot of this substitute loss parameter against equivalent diffusion ratio at minimum loss is shown in figure 14 to illustrate the effectiveness of the parameter. As in the case of the  $(\theta/c)_2$  correlations, it was necessary to use faired values of  $\bar{w}_1$  when local laminar separation effects were apparent. (Differences between the  $(\theta/c)_2$  correlations of fig. 7 and the  $\Omega$  correlations of fig. 14 are therefore due to possible differences in the respective fairing processes as well as to the neglected terms in eq. (10).) The values of total-pressure-loss parameter in figure 14 are mass-averaged values.



## DISCUSSION OF RESULTS

## Significance of Correlations

The correlations of wake momentum thickness  $(\theta/c)_2$  with upper-surface diffusion ratio  $V_{\max}/V_{0,2}$  obtained for the available cascade data in figures 6 and 7 are considered to indicate an essential confirmation of the basic diffusion hypothesis for values of diffusion ratio less than about 2.0. This is based on the observation that, for each family of blades, with minor exceptions, a well-defined relationship independent of solidity, stagger angle, or camber is obtained between  $(\theta/c)_2$  and  $V_{\max}/V_{0,2}$ . (The poor correlation observed for some of the 65-(C<sub>10</sub>A<sub>2</sub>I<sub>8b</sub>)10 blades at higher than minimum-loss angles of attack in figure 7(b), as discussed on p. 11, may not necessarily constitute a violation of the hypothesis.) Fundamentally, these results (within their limitations), as well as the results of references 5 and 6, suggest that the first-order determinant of the boundary-layer growth resulting from a diffusion in velocity on a conventional airfoil surface is the over-all diffusion on the surface  $V_{\max}/V_{0,2}$  rather than the specific velocity distribution, at least for values of diffusion ratio up to about 2.

The failure of the data for the 65-(12A<sub>6</sub>I<sub>4</sub>)10 blade to fall within the limits of  $(\theta/c)_2$  of all the other blades in figure 6(b) (attributed to a more favorable lower-surface velocity distribution) indicates that the magnitude of the values of  $(\theta/c)_2$  in the diffusion correlation for a given blade family will also depend, at least at minimum loss, on the diffusion on the lower surface. The development of a universal diffusion correlation covering a wide range of blade families might require a more complete analysis in which the diffusion hypothesis is applied to both the upper and lower surfaces separately. The available loss data, however, do not permit an evaluation of the individual boundary-layer contributions from each surface.

The essentially universal correlations obtained for  $(\theta/c)_2$  when plotted against equivalent diffusion ratio  $D_{eq}$  in figures 9 and 13 may be of considerable practical value in that they provide a means of estimating theoretically the magnitude of the loss in total pressure and the stall regions of conventional blade sections such as those analyzed herein. Examples of the use of these plots for such purposes are considered in the following sections.

## Estimation of Total-Pressure Loss

As developed in reference 1 (from eq. (10)), the total-pressure-loss coefficient at the cascade measuring station is given by

$$\bar{\omega}_1 = 2 \left( \frac{\theta}{c} \right)_2 \frac{\sigma}{\cos \beta_2} \left( \frac{\cos \beta_1}{\cos \beta_2} \right)^2 \left[ 1 - \left( \frac{\theta}{c} \right)_2 \frac{\sigma H_2}{\cos \beta_2} \right]^{-3} \left( \frac{2H_2}{3H_2 - 1} \right) \quad (12)$$

in which, for conventional measuring-station locations of about  $x/c = 1.0$  to 1.5,  $H_2$  can be taken constant at 1.08 (appendix D). Thus, for a blade of given solidity and air inlet and outlet angles, the loss in total pressure can be calculated if the momentum thickness is known. The wake momentum thickness  $(\theta/c)_2$ , however, can be estimated from representative empirical variations of  $(\theta/c)_2$  against  $D_{eq}$  obtained from the data correlations of figures 9 and 13. For example, for calculation purposes, a representative average curve for  $(\theta/c)_2^*$  at minimum loss can be established from figure 9 as shown in figure 15. The calculation of  $D_{eq}^*$  (from eq. (5)) from the given values of  $\sigma$ ,  $\beta_1$ , and  $\beta_2$  then yields  $(\theta/c)_2^*$  from figure 15 and  $\bar{\omega}_1$  from equation (12).

Illustrative calculations of the variations of minimum-loss total-pressure-loss coefficient  $\bar{\omega}_1^*$  with blade solidity  $\sigma$  obtained from this procedure are shown in figure 16 for a range of values of air inlet angle  $\beta_1$  and air turning angle  $\Delta\beta^* (\beta_2 = \beta_1 - \Delta\beta)$ . The sharp rise in loss coefficient at the lower solidity values in figure 16 is a result of the rapid increase in diffusion ratio as solidity is reduced. The circles on the curves indicate the points at which the diffusion ratio is equal to 2.0. (At  $\beta_1 = 60^\circ$ ,  $D_{eq}^*$  is greater than 2.0 at all solidities for  $\Delta\beta^* = 30^\circ$  and  $40^\circ$ , fig. 16(c).)

In a similar manner, procedures can be established for estimating the total-pressure loss at angles of attack greater than the minimum-loss point by the use of representative momentum-thickness - diffusion curves from figure 7 or from figure 13 and the equivalent diffusion ratio of equation (8).

When cascade blade sections are used as the elements of a compressor stage, the magnitude of the minimum-loss coefficient is not the sole measure of the effectiveness of the section. The section adiabatic efficiency, for example, will depend also on the work input across the element and the dynamic head of the relative inflow. Furthermore, the selection of a design solidity will generally also be based on consideration of the unstalled or useful range of operation of the section, since this factor will also vary with solidity. The influence of solidity on the unstalled range of a blade is illustrated in a later section.

### Blade Stall

Various concepts and definitions of blade stall have been used in cascade practice. In general, blade stall refers to the condition where

a marked deterioration of the flow occurs as a result of the growth or separation of the boundary layer on one of the blade surfaces. Specifically, blade stall has been defined to occur, for example, when the loss attains twice its minimum value, when a relatively marked decrease in turning angle is observed, or when a certain rate of increase in loss is attained. A more universal indication of blade stall is suggested by the correlations presented in figures 6, 7, 9, and 13, if the high values of  $(\theta/c)_2$  at  $V_{\max}/V_{0,2}$  or  $Deq$  greater than about 2 are interpreted as representing stalled flow. Thus, a stalling criterion at minimum loss as well as at greater angles of attack can be established as the upper-surface diffusion ratio in either its specific or equivalent form (eq. (8)). The stalling diffusion ratio, defined herein as the value of  $Deq$  above which a large rise in loss is possible for these blades, is indicated to be about 2 for all the low-speed data considered. The value of 2 can also be adopted as the stalling ratio in terms of measured  $V_{\max}/V_{0,2}$  for all blades if the deviations of the data for the 65-( $C_{l0}A_{218b}$ )10 blades in figure 7(b) can be discounted. This limiting value of  $V_{\max}/V_{0,2}$  for 65-( $C_{l0}A_{10}$ )10 blades is in agreement with the results obtained in reference 7.

A comparable indication of the lower-surface diffusion ratio associated with blade stall at low angles of attack (negative stall) could not be investigated because the available data did not show lower-surface peak velocities considerably greater than the upper-surface peak velocities. However, it is believed that a similar limiting diffusion ratio exists for the lower surface at negative stall.

#### Estimation of Unstalled Range

The equations for equivalent diffusion ratio developed in the empirical analysis can be used to obtain an estimate of the low-speed unstalled range of operation of conventional blade sections. At the stalled condition, from equation (8),

$$Deq,s = \frac{\cos \beta_{2,s}}{\cos \beta_{1,s}} \left[ 1.12 + s(\alpha_s - \alpha^*)^{1.43} + 0.61 \frac{\cos^2 \beta_{1,s}}{\sigma} (\tan \beta_{1,s} - \tan \beta_{2,s}) \right] \quad (13)$$

where  $\alpha_s - \alpha^*$  is the angle-of-attack range from reference minimum loss to positive stall, hereinafter called the half range. For cascade operation at fixed air inlet angle, the equivalent diffusion ratio at stall  $Deq,s$  can be expressed in terms of conditions at minimum loss (from eq. (9)) as

$$Deq,s = \frac{\cos \left[ \beta_2^* - \frac{d(\Delta \beta^*)}{d\alpha} (\alpha_s - \alpha^*) \right]}{\cos \beta_1^*} \left( 1.12 + s(\alpha_s - \alpha^*)^{1.43} + 0.61 \frac{\cos^2 \beta_1^*}{\sigma} \left\{ \tan \beta_1^* - \tan \left[ \beta_2^* - \frac{d(\Delta \beta^*)}{d\alpha} (\alpha_s - \alpha^*) \right] \right\} \right) \quad (14)$$

Thus, for a fixed value of  $D_{eq,s}$  and given values of  $\beta_1^*$  and  $\sigma$ , the half range  $\alpha_s - \alpha^*$  can be computed as a function of  $\beta_2^*$  and consequently  $\Delta\beta^*$ . Calculated variations of half range with  $\Delta\beta^*$  and  $\sigma$  are shown in figure 17 for  $D_{eq,s} = 2.0$  and  $a = 0.0117$ .

The unstalled half range can also be determined as a function of the diffusion level at minimum loss, since  $D_{eq}^*$  (eq. (5)) can be computed from the quantities in equation (14). Plots of  $\alpha_s - \alpha^*$  against  $D_{eq}^*$  for  $D_{eq} = 2.0$  and  $a = 0.0117$  are shown in figure 18 to illustrate the effect of minimum-loss or "design" diffusion on unstalled range at fixed air inlet angle.

If the values of half range obtained are multiplied by 2, the range of angle of attack from positive stall to a value of equal total-pressure-loss coefficient on the low-angle side is obtained. Furthermore, if this point at low  $\alpha$  can be regarded as the point of negative stall, then the complete unstalled range of operation can be obtained from equations (13) and (14).

In the present calculations, blade stall was taken to occur at a diffusion ratio of 2.0, since it represented the region of possible large rise in loss. In many cases (figs. 7 and 13), however, considerably larger values of diffusion ratio were noted without any sudden rise in loss. A potential for increasing the unstalled range of operation of cascade sections may therefore exist, if the various factors affecting the loss variation in this region can be determined and controlled.

#### Limitations and Restrictions

The results obtained from the loss correlations presented herein necessarily contain several limitations and restrictions pertaining to the blade surface velocity distributions (as affected by blade shape and maximum thickness), the flow Reynolds number, the flow inlet Mach number, and the two-dimensionality of the flow. It is desirable that these limitations be kept in mind in any application or extension of the results.

Blade shape. - An important factor determined by blade shape (i.e., thickness and mean-camber-line distributions) that was revealed to influence the correlation of momentum thickness with upper-surface diffusion ratio is the lower-surface velocity distribution. The influence of a more favorable lower-surface diffusion in producing a smaller wake momentum thickness for a given value of upper-surface diffusion ratio has already been noted in the correlation for the 65-(12A<sub>6</sub>I<sub>4</sub>)10 blade at minimum loss

in figure 6(b). Thus, blade shapes that produce lower-surface velocity distributions markedly different from those of the reference blades may not experience similar upper-surface diffusion correlations. The effect of different lower-surface diffusion, however, will generally tend to decrease with increasing angle of attack or diffusion ratio because of the reduced contribution of the lower-surface flow to the total blade wake for these conditions.

It might also be expected that the chordwise location of the upper-surface peak velocity affects the diffusion correlation because of the variation in initial boundary-layer state that might occur at the start of the diffusion. Although the peak velocities in the data were observed to occur between the leading edge and the midchord point at minimum-loss angle of attack, no distinguishable trends could be noted that were due to these different locations. However, this may not always be the case.

Finally, it is noted that the correlations in terms of equivalent diffusion ratio (figs. 9 and 13) do not appear to be sensitive to blade shape because of the previously discussed compensating effects of the relation between the measured and empirical values of  $V_{max}/V_1$  (fig. 8(b)).

Maximum thickness. - The empirical correlations as well as the previous discussions are based on blades of a fixed ratio of maximum-thickness to chord length of 0.10. Theoretically, the loss and stall characteristics of a blade section will vary with maximum blade-thickness because of the influence of the thickness on the maximum surface velocities.

At minimum loss, the variation of calculated  $(\theta/c)_2$  with measured upper-surface  $V_{max}/V_{O,2}$  for the loss data of reference 16 indicates an increase in wake momentum thickness with blade maximum thickness as shown in figure 19. Apparently, factors other than the increased upper-surface diffusion ratio (i.e., poorer lower-surface velocity distribution and larger trailing-edge thickness ratio) are involved in the increase in minimum-loss  $(\theta/c)_2$  with maximum thickness. These data suggest that, for purposes of loss estimation, a family of representative curves of  $(\theta/c)_2$  against  $V_{max}/V_{O,2}$  may be constructed for various maximum thickness, in which the minimum-loss diffusion ratio for all thickness is calculated as before for the 10-percent-thick section (eq. (5)).

It is further noted in the limited experimental data of reference 16 that the value of  $V_{max}/V_{O,2}$  at which a sharp rise in  $(\theta/c)_2$  occurs tends to increase as maximum thickness is reduced. However, since the rate of increase of  $V_{max}/V_{O,2}$  with  $\alpha$  tends to increase with reduced thickness, a net decrease in unstalled range is obtained as maximum thickness is decreased for these data.

In view of the presence of irregularities in the data of reference 16 due to local laminar separation effects, however, it is not known to what extent the specific changes in loss and stall characteristics observed for the changes in maximum thickness of the 65-(12A<sub>10</sub>)10 blade in reference 16 represent universal trends for all cascade sections. General maximum-thickness corrections to the loss and stall characteristics of the 10-percent-thick sections as derived herein are therefore not currently indicated.

Reynolds number. - Since the loss and stall characteristics of cascade sections depend on the surface boundary-layer development, it is expected that these characteristics will be influenced by such factors as blade-chord Reynolds number, free-stream turbulence, and blade surface roughness. The data of the present analysis are restricted to Reynolds numbers between  $2.0 \times 10^5$  and  $4.45 \times 10^5$ . It is presumed that reduced wake momentum thicknesses and possibly larger values of stalling diffusion ratio will occur at higher Reynolds numbers and turbulence levels (especially if local laminar separation effects are no longer present), but no specific indication of the magnitudes involved is available.

Suction-surface diffusion ratios at separation for isolated airfoils were found to be between 2.3 and 2.9 at a chord Reynolds number of  $6 \times 10^6$  in reference 6. However, since the definition of separation in reference 6 may not correspond to the definition of stall considered herein, it is not known to what extent this apparent increase in stalling diffusion ratio compared with the cascade airfoil can be attributed to increased Reynolds number.

Compressibility. - It is well known that, as inlet Mach number increases, compressibility causes an increase in the surface diffusion ratios of a given cascade configuration. Increased wake thickness and reduced range of unstalled operation result. The low-speed correlations obtained herein are therefore not representative of high Mach number performance.

Specifically, an extension of the current correlation approach to high subsonic Mach numbers (in absence of shock waves) will involve the establishment of further empirical relations for  $V_{\max}/V_1$  over a range of inlet Mach numbers. The compressibility effect on the  $V_1/V_{0,2}$  ratio (axial velocities are no longer equal at inlet and outlet in a compressible cascade flow) must also be accounted for, and a compressible relation between  $(\theta/c)_2$  and  $\bar{\omega}_1$  needs to be derived.

When shock waves are present on the blade surfaces at high subsonic Mach numbers, the theoretical low-speed model of the outlet flow as established in figure 2 is no longer applicable. Free-stream total pressure is no longer constant across the blade spacing, and the location of the points of maximum velocity can vary considerably along the surface,

depending on blade solidity, stagger, and back pressure. In such event, the presence of generally greater initial boundary-layer thicknesses and possible complex interaction phenomena at the start of the velocity diffusion requires a complete reevaluation of the diffusion concept and relations. Furthermore, in the presence of shock waves, the substitute mass-averaged total-pressure-loss parameter  $\Sigma$  of equation (11) will no longer represent the blade-wake momentum thickness.

Two-dimensionality. - Another limitation of the derived correlations pertains to their applicability primarily to two-dimensional flows. In axial-flow blade rows, various three-dimensional effects such as secondary flows, spanwise boundary-layer flows, and changes in ratio of inlet to outlet axial velocity and streamline radius occur which can materially affect the loss and stall relations of a given blade section. In an elementary way, changes in axial velocity ratio can be introduced in the current expressions for equivalent diffusion ratio by considering now that

$$\frac{V_1}{V_{0,2}} = \frac{\cos \beta_2}{\cos \beta_1} \frac{V_{z,1}}{V_{0,z,2}} \quad (15)$$

Similarly, change in streamline radius across the section can be included by considering the circulation term in terms of  $r_2 V_{y,2}$  and  $r_1 V_{y,1}$ . However, only comparative experimental investigations can indicate to what extent the current loss and stall relations can be effectively applied to sections in compressor blade rows.

#### SUMMARY OF RESULTS

The preceding analysis of low-speed-cascade data has shown that significant experimental correlation between loss and velocity diffusion can be obtained for several conventional 10-percent-thick low-speed compressor blade sections if the loss is expressed in terms of the ratio of wake momentum thickness to chord length and the diffusion is expressed in terms of the ratio of measured maximum upper-surface velocity to outlet velocity. A well-defined relationship between wake momentum thickness and upper-surface diffusion ratio was obtained for a wide range of blade configurations for values of diffusion ratio up to about 2 in most cases, after which a wide scatter of the data is observed. It was also indicated that the form of the lower-surface velocity distribution and the magnitude of the maximum blade thickness can influence the magnitude of the proportionality between wake momentum thickness and upper-surface diffusion ratio. Fundamentally, these results (within their limitations) suggest that the first-order determinant of the boundary-layer growth resulting from a diffusion in velocity on a conventional blade surface is the over-all diffusion on the surface  $V_{\max}/V_{0,2}$  rather than the specific velocity distribution, at least for values of diffusion ratio up to about 2.

From derived empirical relations, it was possible to establish an equivalent diffusion ratio expressible in terms of the velocity triangle and blade solidity. Within the restrictions of the data (range of blade configurations tested, range of Reynolds number, low-speed two-dimensional flow), an essentially universal correlation between wake momentum thickness and equivalent diffusion ratio was obtained at angles of attack at minimum loss and greater for all blade configurations. The possibility of blade stall at minimum-loss and greater angles of attack, as evidenced by a sharp rise in wake momentum thickness, was indicated to occur whenever the equivalent diffusion ratio attains a value of about 2.

With the use of the equivalent diffusion ratio, means for estimating the low-speed total-pressure loss and the unstalled range of operation of similar conventional cascade sections as functions of solidity, air inlet angle, and air turning angle were established. Calculations showed that minimum total-pressure loss generally decreased with decreasing solidity until a value was reached at which the diffusion becomes excessive, and the loss then rises sharply. For normal design ranges, the lowest values of total-pressure loss occurred at solidities less than unity. The range of angle of attack from minimum loss to positive stall was found to be a primary function of the equivalent diffusion ratio at minimum loss, calculated range decreasing with increasing minimum-loss diffusion ratio.

Lewis Flight Propulsion Laboratory  
National Advisory Committee for Aeronautics  
Cleveland, Ohio, November 23, 1956



## APPENDIX A

## CALCULATION OF MOMENTUM THICKNESS FROM WAKE FORCE COEFFICIENT

The wake force coefficient  $C_{w,1}$  is defined in terms of inlet dynamic head (ref. 9) as

$$C_{w,1} = \frac{F_w}{\frac{1}{2}\rho V_1^2 c} \quad (A1)$$

where  $F_w$  is the wake momentum force per unit span expressing the momentum difference between the free-stream flow and the wake flow. From equation (6) of reference 9 (using the coordinate system of fig. 1),

$$F_w = \int_{-s/2}^{s/2} \rho V_{z,2} (V_{0,2} - V_2) dy \quad (A2)$$

where the subscript 0 refers to free-stream conditions outside the wake. Substitution of equation (A2) into equation (A1) for constant angle across the wake then yields

$$C_{w,1} = \frac{\frac{2}{c} \cos \beta_2 \int_{-s/2}^{s/2} \frac{V_2}{V_{0,2}} \left(1 - \frac{V_2}{V_{0,2}}\right) dy}{\left(\frac{V_1}{V_{0,2}}\right)^2} \quad (A3)$$

Since the free-stream velocity is constant between the wakes in the plane of the measuring station (fig. 2), the integral term in equation (A3) is the wake momentum thickness  $\theta_y$ . Thus, equation (A3) becomes

$$C_{w,1} = 2 \left(\frac{V_{0,2}}{V_1}\right)^2 \cos \beta_2 \left(\frac{\theta_y}{c}\right)_2 \quad (A4)$$

Since the plane of integration in the equation developments (cascade outlet measuring station) is sufficiently far downstream (of the order of 1 to 1.5 chord lengths behind the blade), changes in wake characteristics along the direction of flow will be very small (ref. 2). Consequently, the wake thicknesses normal to the axial direction (subscript

y) can be expressed as the conventional thicknesses normal to the outlet flow (no subscript) as

$$\left. \begin{aligned} \theta &= \theta_y \cos \beta_2 \\ \delta &= \delta_y \cos \beta_2 \\ \delta^* &= \delta_y^* \cos \beta_2 \end{aligned} \right\} \quad (A5)$$

Thus, from equations (A4) and (A5), the momentum-thickness ratio is given by

$$\left(\frac{\theta}{c}\right)_2 = \frac{C_{w,1}}{2} \left(\frac{V_1}{V_{0,2}}\right)^2 \quad (A6)$$

Equation (A6) points to one of the major difficulties in the accurate determination of the momentum thickness from the measured loss coefficients, namely, the correct values for free-stream velocity ratio  $V_1/V_{0,2}$  that existed in the various cascade tunnels. Since

$$\left(\frac{V_1}{V_{0,2}}\right)^2 = \left(\frac{V_{z,1}}{V_{0,z,2}}\right)^2 \left(\frac{\cos \beta_2}{\cos \beta_1}\right)^2 \quad (A7)$$

it is seen that the velocity ratio is a function not only of the measured air angles but also of the free-stream axial velocity ratio across the blade. The axial velocity ratio of equation (A7) is a measure of the degree to which two-dimensional flow has been achieved across the cascade. In low-speed flow this ratio is frequently referred to as the cascade contraction ratio. Values of contraction ratio have not generally been identified in conventional cascade performance evaluations. It was therefore necessary in the developments to make an assumption concerning the two-dimensionality of the cascade tunnels in question in order to evaluate the axial velocity ratio. Since good two-dimensionality control was exercised for all of the cascade data (refs. 9 to 12), it was assumed that two-dimensional flow was obtained in the cascade for all configurations.

For two-dimensional incompressible flow with uniform upstream conditions, continuity requires that

$$sV_1 \cos \beta_1 = \cos \beta_2 \int_{-s/2}^{s/2} V_2 dy \quad (A8)$$

Now, equation (A8) can be expressed as

$$sV_1 \left( \frac{\cos \beta_1}{\cos \beta_2} \right) = sV_{0,2} - V_{0,2} \int_{-s/2}^{s/2} \left( 1 - \frac{V_2}{V_{0,2}} \right) dy \quad (A9)$$

so that, with the integral term being equal to the wake displacement thickness  $\delta_y^*$  (fig. 2), it follows that

$$\left( \frac{V_1}{V_{0,2}} \right)^2 = \left( \frac{\cos \beta_2}{\cos \beta_1} \right)^2 \left( 1 - \frac{(\delta_y^*)_2}{s} \right)^2$$

or, from equation (A5) and the definitions of form factor  $H = \delta^*/\theta$  and solidity  $\sigma = c/s$ ,

$$\left( \frac{V_1}{V_{0,2}} \right)^2 = \left( \frac{\cos \beta_2}{\cos \beta_1} \right)^2 \left[ 1 - \left( \frac{\theta}{c} \right)_2 \frac{H_2 \sigma}{\cos \beta_2} \right]^2 \quad (A10)$$

Substitution of equation (A10) into equation (A6) then yields for two-dimensional flow

$$\left( \frac{\theta}{c} \right)_2 = \frac{C_{w,1}}{2} \left( \frac{\cos \beta_2}{\cos \beta_1} \right)^2 \left[ 1 - \left( \frac{\theta}{c} \right)_2 \frac{H_2 \sigma}{\cos \beta_2} \right]^2 \quad (A11)$$

and, by quadratic solution,

$$\left. \begin{aligned} \left( \frac{\theta}{c} \right)_2 &= \frac{C_{w,1} \left( \frac{\cos \beta_2}{\cos \beta_1} \right)^2}{1 + b + \sqrt{1 + 2b}} \\ b &= C_{w,1} \left( \frac{H_2 \sigma}{\cos \beta_2} \right) \left( \frac{\cos \beta_2}{\cos \beta_1} \right)^2 \end{aligned} \right\} \quad (A12)$$

where

For wake coefficients expressed in terms of some other reference condition (e.g., vector mean or outlet conditions), relations equivalent to equation (A12) can be obtained from the use of the equality

$$C_{w,1} = C_{w,ref} \left( \frac{V_{ref}}{V_1} \right)^2 \quad (A13)$$

Values of  $H_2$  used in the calculations of  $(\theta/c)_2$  based on the wake coefficient and the other loss parameters were determined according to the considerations presented in appendix D.

## APPENDIX B

## CALCULATION OF MOMENTUM THICKNESS FROM DRAG COEFFICIENT

The drag coefficient is defined as the ratio of the drag force per unit blade area to some reference dynamic head as

$$C_{D,ref} = \frac{F_D}{\frac{1}{2} \rho V_{ref}^2 c} \quad (B1)$$

where  $F_D$  is the drag force per unit blade span. The drag force in incompressible flow is evaluated as the component of the total force parallel to the vector mean velocity between blade inlet (far upstream) and blade outlet (far downstream), as indicated in figure 20. Reference velocities generally used are the inlet velocity, the outlet velocity, and the vector mean velocity between inlet and outlet. The total blade force is computed from the axial and tangential force components, which are determined from measured velocities and pressures.

In current cascade practice, different methods of calculating the drag force exist, depending on whether the effects of the velocity defect in the blade wake are considered in the evaluation of the total force  $F$  and the vector mean direction  $\beta_m$  (as discussed in ref. 12). In the present analysis, it was necessary to consider that all reported drag coefficients were the theoretically correct values.

Because of the complex relation between the drag force and the tangential and axial force components (which are determined from measured velocities and pressures) at the measuring station, it was not possible to obtain directly a relation between drag coefficient and wake momentum-thickness ratio. Equations for  $(\theta/c)_2$  therefore had to be developed in an indirect manner as follows. Since the drag coefficients are assumed to be the theoretically correct ones, they will be independent of distance behind the blade. Thus, if a point sufficiently far downstream (station subscript  $\infty$ ) is considered such that the wakes have completely mixed with the free-stream flow, the velocities, pressures, and angles will all be uniform across the complete blade spacing.

For uniform outlet conditions, from figure 20, the drag force is given by

$$F_D = F_y \sin \beta_m - F_z \cos \beta_m \quad (B2)$$

Since two-dimensional flow is assumed, the axial velocities at inlet and outlet will be equal. The axial force  $F_z$  then results only from the change in static pressure across the blade, which in the presence of losses is given by

$$F_z = s(p_\infty - p_1) = s \left[ \left( p_\infty - \frac{1}{2} \rho v_\infty^2 \right) - \left( p_1 - \frac{1}{2} \rho v_1^2 \right) \right]$$

or

$$F_z = s \left[ \frac{1}{2} \rho (v_1^2 - v_\infty^2) - (\Delta \bar{P})_\infty \right] \quad (B3)$$

The force in the tangential direction is determined by the momentum change in the tangential direction, or

$$F_y = s \rho v_z (v_{y,1} - v_{y,\infty}) \quad (B4)$$

Equation (B2) then becomes from equations (B3) and (B4)

$$\frac{F_D}{s \cos \beta_m} = \rho v_z (v_{y,1} - v_{y,\infty}) \tan \beta_m - \left[ \frac{1}{2} \rho (v_1^2 - v_\infty^2) - (\Delta \bar{P})_\infty \right] \quad (B5)$$

With (from fig. 20)

$$\tan \beta_m = \frac{v_{y,1} - \frac{1}{2} \Delta v_y}{v_z} = \frac{v_{y,1} + v_{y,\infty}}{2v_z} \quad (B6)$$

and

$$v_1^2 - v_\infty^2 = v_{y,1}^2 - v_{y,\infty}^2$$

substitution of these terms into equation (B5) reduces that equation to

$$\frac{F_D}{s \cos \beta_m} = (\Delta \bar{P})_\infty \quad (B7)$$

Dividing equation (B7) by free-stream dynamic head at the outlet measuring station  $\frac{1}{2} \rho v_{0,2}^2$ , with  $c/s = \sigma$ , gives

$$\frac{\sigma F_D}{\cos \beta_m \frac{1}{2} \rho c v_{0,2}^2} = \frac{(\Delta \bar{P})_\infty}{\frac{1}{2} \rho v_{0,2}^2} = \bar{\omega}_{2,\infty} \quad (B8)$$

By definition, the drag coefficient based on outlet velocity is given by

$$C_{D,2} = \frac{F_D}{\frac{1}{2} \rho V_{0,2}^2}$$

so that, finally,

$$\bar{\omega}_{2,\infty} = \frac{\sigma C_{D,2}}{\cos \beta_m} \quad (B9)$$

From the developments of reference 1, it can be shown that the loss for complete mixing far downstream can be related to the wake momentum-thickness ratio at the measuring station (station 2) by the equation

$$\bar{\omega}_{2,\infty} = \frac{(\Delta \bar{P})_\infty}{\frac{1}{2} \rho V_{0,2}^2} = 2 \left( \frac{\theta}{c} \right)_2 \frac{\sigma}{\cos \beta_2} \left( 1 + \frac{1}{2} \left( \frac{\theta}{c} \right)_2 \frac{\sigma}{\cos \beta_2} \left\{ H_2^2 - \sin^2 \beta_2 \left[ H_2 - \frac{1}{1 - \left( \frac{\theta}{c} \right)_2 \frac{\sigma H_2}{\cos \beta_2}} \right]^2 \right\} \right) \quad (B10)$$

It is further shown in reference 1 that, if the wake form factor is not greater than about 1.2 (which is the case for the cascade data considered herein), the term involving  $\sin^2 \beta_2$  within the braces in equation (B10) can be neglected, so that for practical purposes

$$\bar{\omega}_{2,\infty} = 2 \left( \frac{\theta}{c} \right)_2 \frac{\sigma}{\cos \beta_2} \left[ 1 + \frac{1}{2} \left( \frac{\theta}{c} \right)_2 \frac{\sigma H_2^2}{\cos \beta_2} \right] \quad (B11)$$

From equations (B9) and (B11) it is then found that

$$\left( \frac{\theta}{c} \right)_2 = \frac{\cos \beta_2}{\sigma H_2^2} \left( \sqrt{1 + \frac{\sigma C_{D,2} H_2^2}{\cos \beta_m}} - 1 \right) \quad (B12)$$

Strictly speaking, in equation (B12),  $\beta_m$  is determined in terms of outlet conditions far downstream where complete mixing has occurred (station  $\infty$ ). However, for practical purposes, it was sufficient to assume that  $\beta_\infty = \beta_2$  (ref. 2) so that, from equation (B6),

$$\beta_m = \tan^{-1} \frac{1}{2} (\tan \beta_1 + \tan \beta_2) \quad (B13)$$

For the drag coefficient based on inlet dynamic head, division of equation (B7) by  $\frac{1}{2}\rho V_1^2$  yields

$$\bar{C}_{D,1} = \frac{\sigma C_{D,1}}{\cos \beta_m} \quad (B14)$$

For two-dimensional flow, from reference 1,

$$\bar{C}_{D,1} = 2 \left( \frac{\theta}{c} \right)_2 \frac{\sigma}{\cos \beta_2} \left( \frac{\cos \beta_1}{\cos \beta_2} \right)^2 \left[ 1 + \frac{1}{2} \left( \frac{\theta}{c} \right)_2 \frac{\sigma H_2^2}{\cos \beta_2} \right] \left[ 1 - \left( \frac{\theta}{c} \right)_2 \frac{\sigma H_2}{\cos \beta_2} \right]^{-2} \quad (B15)$$

Substitution of equation (B15) into equation (B14) then permits a quadratic solution for  $(\theta/c)_2$  to give

$$\left. \begin{aligned} \left( \frac{\theta}{c} \right)_2 &= \frac{C_{D,1} \left( \frac{\cos \beta_2}{\cos \beta_m} \right) \left( \frac{\cos \beta_2}{\cos \beta_1} \right)^2}{1 + b + \sqrt{1 + (H_2 + 2)b}} \\ b &= C_{D,1} \left( \frac{\sigma H_2}{\cos \beta_m} \right) \left( \frac{\cos \beta_2}{\cos \beta_1} \right)^2 \end{aligned} \right\} \quad (B16)$$

where

For the drag coefficient based on the vector mean velocity  $V_m$ ,

$$C_{D,m} = C_{D,1} \left( \frac{V_1}{V_m} \right)^2$$

or, since from continuity  $V_1/V_m = \cos \beta_m / \cos \beta_1$ ,

$$C_{D,m} = C_{D,1} \left( \frac{\cos \beta_m}{\cos \beta_1} \right)^2 \quad (B17)$$



The solution for  $(\theta/c)_2$  is then given by

$$\left(\frac{\theta}{c}\right)_2 = \frac{C_{D,m} \left(\frac{\cos \beta_2}{\cos \beta_m}\right)^3}{1 + b + \sqrt{1 + (H_2 + 2)b}}$$

where

$$b = C_{D,m} \left(\frac{\cos \beta_2}{\cos \beta_m}\right)^3 \left(\frac{\sigma_{H_2}}{\cos \beta_2}\right)$$

(B18)

4222

## APPENDIX C

## CALCULATION OF MOMENTUM THICKNESS FROM TOTAL-PRESSURE-LOSS COEFFICIENT

The total-pressure-loss coefficient based on some reference dynamic head is defined in low speed as

$$\bar{\omega}_{\text{ref}} = \frac{(\Delta\bar{P})_2}{\frac{1}{2}\rho V_{\text{ref}}^2} \quad (\text{C1})$$

where  $(\Delta\bar{P})_2$  is the average loss in total pressure up to the cascade measuring station. The average loss in total pressure in the measuring plane is expressed in terms of either an area average given by

$$(\Delta\bar{P})_A = \frac{1}{s} \int_{-s/2}^{s/2} (P_0 - P) dy \quad (\text{C2})$$

or a mass average given by

$$(\Delta\bar{P})_M = \frac{\int_{-s/2}^{s/2} \rho V_z (P_0 - P) dy}{\int_{-s/2}^{s/2} \rho V_z dy} \quad (\text{C3})$$

For reference 1, the mass-averaged total-pressure-loss coefficient based on outlet dynamic head (subscript 2) is given in terms of the wake characteristics at the measuring station by

$$\bar{\omega}_2 = 2 \left( \frac{\theta}{c} \right)_2 \frac{\sigma}{\cos \beta_2} \left( \frac{2H_2}{3H_2 - 1} \right) \left[ 1 - \left( \frac{\theta}{c} \right)_2 \frac{\sigma H_2}{\cos \beta_2} \right]^{-1} \quad (\text{C4})$$

from which is obtained for the momentum-thickness ratio

$$\left( \frac{\theta}{c} \right)_2 = \frac{\cos \beta_2}{H_2 \sigma \left[ 1 + \frac{4}{\bar{\omega}_2 (3H_2 - 1)} \right]} \quad (\text{C5})$$

For loss coefficients based on inlet velocity,

$$\bar{\omega}_1 = \bar{\omega}_2 \left( \frac{V_{0,2}}{V_1} \right)^2 \quad (C6)$$

where the free-stream velocity ratio  $V_{0,2}/V_1$  for two-dimensional flow is evaluated according to equation (A10). Substitution of equation (A10) into equation (C6) and equation (C6) into (C4) then yields

$$\left( \frac{\theta}{c} \right)_2 = \left( \frac{3H_2 - 1}{4H_2} \right) \frac{\cos \beta_2}{\sigma} \left( \frac{\cos \beta_2}{\cos \beta_1} \right)^2 \bar{\omega}_1 \left[ 1 - \left( \frac{\theta}{c} \right)_2 \frac{H_2 \sigma}{\cos \beta_2} \right]^3 \quad (C7)$$

In view of the complicated cubic equation involved in the explicit solution for  $(\theta/c)_2$ , for practical purposes an iteration solution of equation (C7) can be used. For the initial calculation,  $(\theta/c)_2$  within the brackets can be taken to be equal to the product of all the terms outside the brackets in equation (C7). Three iterations are generally sufficient to produce results of acceptable accuracy.

In cascade practice, the loss in total pressure is generally presented as an area average of the defect in total pressure in the wake as defined by equation (C2). It is necessary, therefore, to convert the area-averaged loss to a mass-averaged loss for use in the equations for  $(\theta/c)_2$ , where

$$\bar{\omega}_M = \left( \frac{\bar{\omega}_M}{\bar{\omega}_A} \right) \bar{\omega}_A \quad (C8)$$

Curves of the ratio of mass-averaged to area-averaged total-pressure-loss coefficient  $\bar{\omega}_M/\bar{\omega}_A$  derived from experimental and theoretical considerations were determined in reference 2 as a function of downstream distance  $x/c$  and the ratio of full wake thickness to normal blade spacing  $\delta/s_n$ . The derived ratios are shown in figure 21.

Since values of  $\delta/s_n$  were not known for the available cascade loss data, they can be estimated according to the following considerations. Examination of experimental data showed that the ratio of wake momentum thickness to full thickness could be represented on the average by the curve in figure 22. The derived curve in figure 22 was obtained from the data of reference 2. Values of  $\delta/s_n$  for a given cascade geometry and

x/c location were then obtained from assumed values of  $\theta/c$  from the relation

$$\frac{\delta}{s_n} = \frac{\delta}{c} \frac{\sigma}{\cos \beta_2} = \frac{\frac{\theta}{c} \frac{\sigma}{\cos \beta_2}}{\frac{\theta}{c}} \quad (C9)$$

in conjunction with figure 22. Several trial values of  $\theta/c$  are used to determine trial values of  $\bar{a}_M/\bar{a}_A$  in the calculation of  $\theta/c$ . Correspondence of the trial and computed values of  $\theta/c$  then determines the correct value of  $\theta/c$ .

4222

r CP-5 back

## APPENDIX D

## WAKE FORM FACTOR

In the absence of specific experimental data concerning the magnitudes of the wake form factors encountered in cascade flow, it was necessary to assume representative values of  $H_2$  for use in the calculation of  $(\theta/c)_2$  over the range of interest of the various cascade sections. Reference 2 showed empirically that cascade wake form factor  $H$  decreases rapidly with distance downstream of the cascade  $x/c$  depending on the initial value of form factor at the trailing edge  $H_{te}$ . For a range of values of  $H_{te}$  from 1.4 to 3.0 (representing zero diffusion flow to badly separated flow), the corresponding range of values of  $H$  was quite small at the conventional measuring-station locations of  $x/c = 1$  and 1.5. The possibility of using one average value of  $H_2$  at a given station location over a wide range of cascade geometries and angles of attack (and consequently  $H_{te}$ ) was therefore suggested. Examination of the various conversion equations used and the limits of variation of  $H_2$  given by the empirical relations of reference 2 revealed that errors of about  $\pm 1$  percent or less in the magnitude of  $(\theta/c)_2$  might be introduced by the use of a constant value of  $H_2$  at a given station location for the loss data considered. Values of  $H_2$  selected for the calculations of  $(\theta/c)_2$  were 1.08 at  $x/c = 1$  and 1.07 at  $x/c = 1.5$ .

4222

## APPENDIX E

## CALCULATION OF TOTAL-PRESSURE-LOSS COEFFICIENT

For the computations of total-pressure-loss coefficient from measured drag coefficients, it was noted from the results of reference 2 that, at the measuring-station locations of the available cascade data (1 to 1.5 chord lengths downstream), the total-pressure-loss coefficient at the station  $\bar{\omega}_1$  should be very nearly equal to the loss for complete mixing  $\bar{\omega}_{1,\infty}$ . Thus, the total-pressure-loss coefficient at the measuring station was determined from equation (B14) and (B18) as

$$\bar{\omega}_1 = \frac{\sigma C_{D,1}}{\cos \beta_m} \quad (E1)$$

and

$$\bar{\omega}_1 = \frac{\sigma C_{D,m}}{\cos \beta_m} \left( \frac{\cos \beta_1}{\cos \beta_m} \right)^2 \quad (E2)$$

## REFERENCES

1. Lieblein, Seymour, and Roudebush, William H.: Theoretical Loss Relations for Low-Speed Two-Dimensional-Cascade Flow. NACA TN 3662, 1956.
2. Lieblein, Seymour, and Roudebush, William H.: Low-Speed Wake Characteristics of Two-Dimensional Cascade and Isolated Airfoil Sections. NACA TN 3771, 1956.
3. Wislicenus, George F.: Fluid Mechanics of Turbomachinery. McGraw-Hill Book Co., Inc., 1947, p. 345.
4. Howell, A. R.: The Present Basis of Axial Flow Compressor Design. Pt. I. Cascade Theory and Performance. British R.&M. No. 2095, British A.R.C., June 1942.
5. Ross, Donald, and Robertson, J. M.: An Empirical Method for Calculation of the Growth of a Turbulent Boundary Layer. Jour. Aero. Sci., vol. 21, No. 5, May 1954, pp. 355-358.
6. Loftin, Laurence K., Jr., and Von Doenhoff, Albert E.: Exploratory Investigation at High and Low Subsonic Mach Numbers of Two Experimental 6-Percent-Thick Airfoil Sections Designed to Have High Maximum Lift Coefficients. NACA RM L51F06, 1951.

7. Savage, Melvyn: Analysis of Aerodynamic Blade-Loading-Limit Parameters for NACA 65- $(C_{70}A_{10})_{10}$  Compressor-Blade Sections at Low Speeds. NACA RM L54L02a, 1955.
8. Lieblein, Seymour, Schwenk, Francis C., and Broderick, Robert L.: Diffusion Factor for Estimating Losses and Limiting Blade Loading in Axial-Flow-Compressor Blade Elements. NACA RM E53D01, 1953.
9. Herrig, L. Joseph, Emery, James C., and Irwin, John R.: Systematic Two-Dimensional Cascade Tests of NACA 65-Series Compressor Blades at Low Speeds. NACA RM L51G31, 1951.
10. Erwin, John R., Savage, Melvyn, and Emery, James C.: Two-Dimensional Low-Speed Cascade Investigation of NACA Compressor Blade Sections Having a Systematic Variation in Mean-Line Loading. NACA TN 3817, 1956.
11. Blight, F. G., and Howard, W.: Tests on Four Aerofoil Cascades. Pt. I - Deflection, Drag, and Velocity Distribution. Rep. E.74, Aero. Res. Labs., Dept. Supply, Melbourne (Australia), July 1952.
12. Felix, A. Richard, and Emery, James C.: A Comparison of Typical National Gas Turbine Establishment and NACA Axial-Flow Compressor Blade Sections in Cascade at Low Speed. NACA RM L53B26a, 1953.
13. Schlichting, H.: Lecture Series "Boundary Layer Theory." Pt. II - Turbulent Flows. NACA TM 1218, 1949.
14. Erwin, John R., and Yacobi, Laura A.: Method of Estimating the Incompressible-Flow Pressure Distribution of Compressor Blade Sections at Design Angle of Attack. NACA RM L53F17, 1953.
15. Carter, A. D. S., and Hughes, Hazel P.: A Theoretical Investigation into the Effect of Profile Shape on the Performance of Aerofoils in Cascade. R.&M. No. 2384, British A.R.C., Mar. 1946.
16. Herrig, L. Joseph, Emery, James C., and Erwin, John R.: Effect of Section Thickness and Trailing-Edge Radius on the Performance of NACA 65-Series Compressor Blades in Cascade at Low Speeds. NACA RM L51J16, 1951.

TABLE I. - BLADE CONFIGURATION AND CASCADE TUNNEL DATA

Blade	1		2	3	4	5	6
Blade type	NACA 65-(010A10)10		10C.4/30C50	10C.4/31C50	65-(010A2Igb)10	65-(12A6I4b)10	65-(12A6I4)10
Reference	9		11	12	10	10	10
Loss parameter of data	$C_{w,1}$ and $C_{D,1}$		$C_{D,1}$	$C_{D,m}$	$C_{w,1}$ and $C_{D,1}$	$C_{w,1}$ and $C_{D,1}$	$C_{w,1}$ and $C_{D,1}$
Air inlet angle, $\beta_1$ , deg	30, 45, 60, 70		30, 45, 60	Variable	30, 45, 60	45, 60	45, 60
Blade-chord angle, $\gamma^0$ , deg	Variable		Variable	29.5	Variable	Variable	Variable
Solidity, $\sigma$	0.5, 0.75	1.0, 1.25, 1.5	1.0	1.0	1.0, 1.5	1.0, 1.5	1.0, 1.5
Chord length, $c$ , in.	2.5	5.0	5.0	4.0	5.0	5.0	5.0
Aspect ratio, $\alpha$	2	1	1	6	1	1	1
Chord Reynolds number, $Re_c$	$2.0 \times 10^5$	$2.45 \times 10^5$	$2.35 \times 10^5$	$2.16 \times 10^5$	$4.44 \times 10^5$	$3.46 \times 10^5$	$3.46 \times 10^5$
Inlet velocity, $V_1$ , ft/sec	150	95	90	120	165	135	135
Tunnel	NACA 5-in. low-speed			Australian low-speed	NACA 5-in. low-speed		
Boundary-layer control	End and side porous-wall suction; side wall slot suction			Side wall slot suction	End and side porous-wall suction; side wall slot suction		
Turbulence factor	1.2		1.2	1.12	Turbulence screens added		
Measuring-station location, $x/c$	1		1	1.5	1	1	1



TABLE II. - ANGLE OF ATTACK AND TURNING ANGLE

AT REFERENCE MINIMUM LOSS

(a) NACA 65-( $C_{L0}A_{10}$ )10 blades of reference 9 (blade 1)

Solidity, $\sigma$	Design lift coeffi- cient, $C_{L0}$	$\beta_1 = 30^\circ$		$\beta_1 = 45^\circ$		$\beta_1 = 60^\circ$		$\beta_1 = 70^\circ$	
		$\alpha^*$ , deg	$\Delta\beta^*$ , deg	$\alpha^*$ , deg	$\Delta\beta^*$ , deg	$\alpha^*$ , deg	$\Delta\beta^*$ , deg	$\alpha^*$ , deg	$\Delta\beta^*$ , deg
0.5	4	----	----	4.5	4.0	4.0	3.0	----	----
	12	----	----	10.1	12.2	7.7	8.7	----	----
	18	----	----	12.0	16.8	10.0	13.0	----	----
0.75	4	----	----	6.1	6.0	6.1	4.8	----	----
	12	----	----	12.1	16.6	10.6	14.3	----	----
	18	----	----	17.5	26.2	14.5	20.2	----	----
1.00	0	3.0	2.3	3.5	1.8	5.0	1.8	5.5	2.6
	4	7.1	9.5	7.1	8.7	7.5	7.7	7.1	6.6
	8	10.7	16.0	9.6	15.2	10.2	12.8	8.2	9.4
	12	14.6	23.1	13.6	20.9	13.6	18.6	10.6	13.3
	15	17.8	29.2	17.3	26.8	14.3	21.7	10.3	15.2
	18	20.5	33.7	18.0	29.6	15.0	23.2	----	----
	21	----	----	21.1	34.5	17.6	26.3	----	----
	24	----	----	24.2	39.6	----	----	----	----
	27	----	----	26.2	42.6	----	----	----	----
1.25	4	8.0	10.6	8.5	10.2	9.5	8.9	8.0	6.8
	8	----	----	----	----	----	----	10.7	12.2
	12	16.6	26.0	16.6	24.7	16.1	21.4	12.6	15.9
	15	----	----	----	----	----	----	13.3	17.9
1.50	18	22.5	37.2	22.5	34.9	19.0	28.0	----	----
	0	4.0	3.4	5.0	3.7	7.0	3.7	8.0	2.7
	4	8.5	11.6	9.1	11.6	10.0	11.6	10.0	8.2
	8	13.2	19.8	12.6	18.7	13.6	18.7	12.2	13.3
	12	19.1	30.0	17.6	26.8	18.1	26.8	14.5	18.6
	15	21.2	34.8	20.8	33.0	18.7	33.0	16.8	21.0
	18	24.0	41.0	24.5	38.9	22.5	38.9	----	----
	21	----	----	26.6	43.7	23.6	43.7	----	----
	24	----	----	28.2	48.0	25.7	48.0	----	----

4232

TABLE II. - Concluded. ANGLE OF ATTACK AND TURNING ANGLE

AT REFERENCE MINIMUM LOSS

(b) NACA 65-(AI)10 blades of reference 10

Blade	Solidity, $\sigma$	Design lift coeffi- cient, $C_{l0}$	$\beta_1 = 30^\circ$		$\beta_1 = 45^\circ$		$\beta_1 = 60^\circ$	
			$\alpha^*$ , deg	$\Delta\beta^*$ , deg	$\alpha^*$ , deg	$\Delta\beta^*$ , deg	$\alpha^*$ , deg	$\Delta\beta^*$ , deg
4 ( $C_{l0}A_2I_{8b}$ )	1.0	4	6.6	9.3	8.8	10.0	6.7	7.7
		8	8.1	14.5	9.0	14.0	8.2	12.2
		12	9.8	21.4	9.8	18.2	8.4	15.2
		18	13.0	29.0	12.4	25.2	12.4	21.1
	1.5	4	8.5	12.2	10.4	13.0	10.9	11.5
		8	10.4	18.9	12.0	19.4	12.9	17.2
		12	12.0	26.3	13.8	25.5	12.5	21.0
		18	16.0	38.0	16.4	34.3	16.0	28.3
5 ( $C_{l0}A_6I_{4b}$ )	1.0	12	----	----	----	----	11.0	15.8
	1.5	12	----	----	17.2	26.3	----	----
6 ( $C_{l0}A_6I_4$ )	1.0	12	----	----	----	----	15.2	18.0
	1.5	12	----	----	21.0	27.7	----	----

(c) C.4 Circular-arc blades of references 11 and 12

Blade	Air inlet angle, $\beta_1^*$ , deg	Angle of attack, $\alpha^*$ , deg	Air turning angle, $\Delta\beta^*$ , deg
2 (10C.4/30C50)	30	14.5	20.6
	45	14.0	19.7
	60	13.0	16.8
3 (10C.4/31C50)	42.3	12.8	19.0

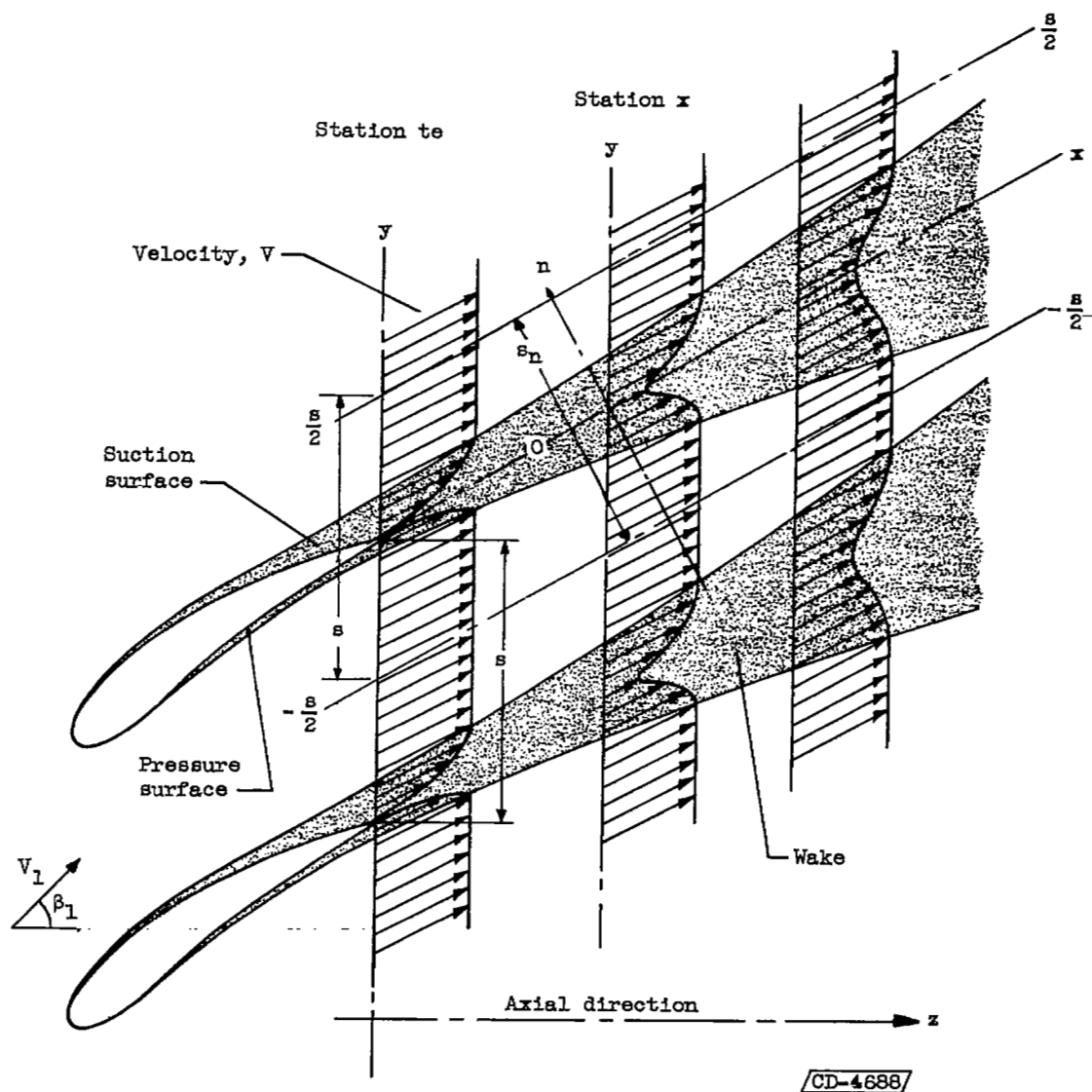
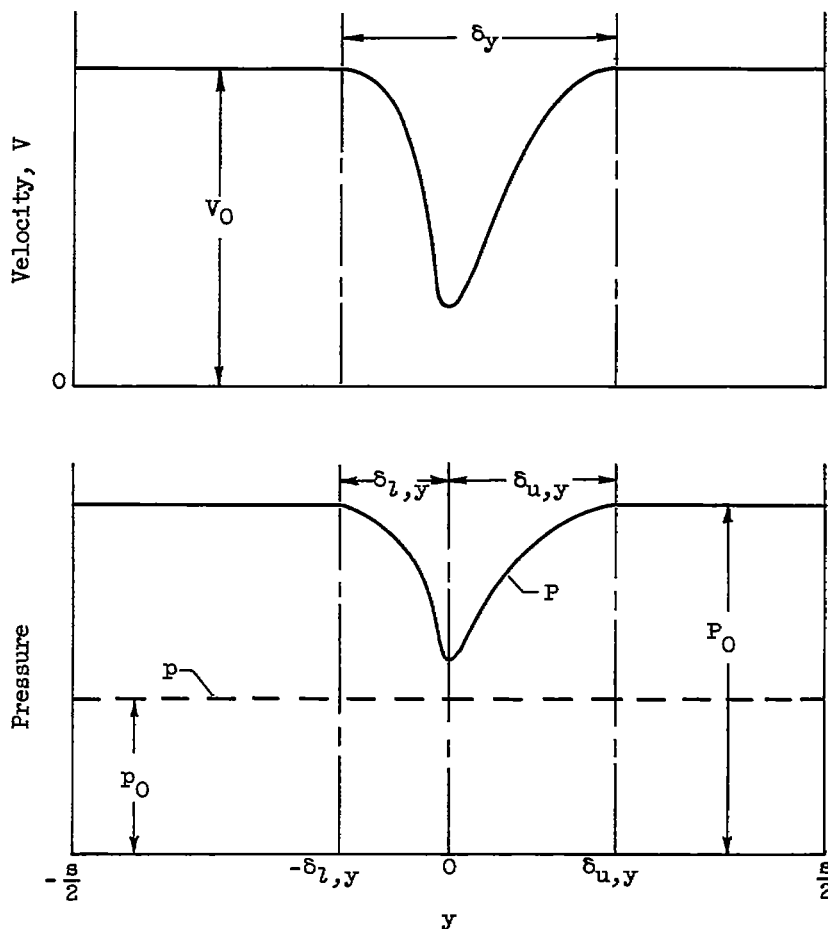


Figure 1. - Schematic representation of wake development in flow about cascade blade sections.



Displacement thickness:  $\delta_y^* = \delta_{u,y}^* + \delta_{l,y}^* = \int_{-\delta_{l,y}}^{\delta_{u,y}} \left(1 - \frac{v}{V_0}\right) dy;$

$$\delta^* = \delta_u^* + \delta_l^* = \delta_y^* \cos \beta$$

Momentum thickness:  $\theta_y = \theta_{u,y} + \theta_{l,y} = \int_{-\delta_{l,y}}^{\delta_{u,y}} \left(1 - \frac{v}{V_0}\right) \frac{v}{V_0} dy;$

$$\theta = \theta_u + \theta_l = \theta_y \cos \beta$$

$$H = \frac{\delta^*}{\theta} = \frac{\delta_y^*}{\theta_y}, \quad \delta = \delta_u + \delta_l = \delta_y \cos \beta$$

Figure 2. - Model variation of velocity and pressure in plane normal to axial direction and definitions of wake properties. (Subscript y refers to properties in plane normal to axial direction; no subscript indicates properties in plane normal to outlet flow.)

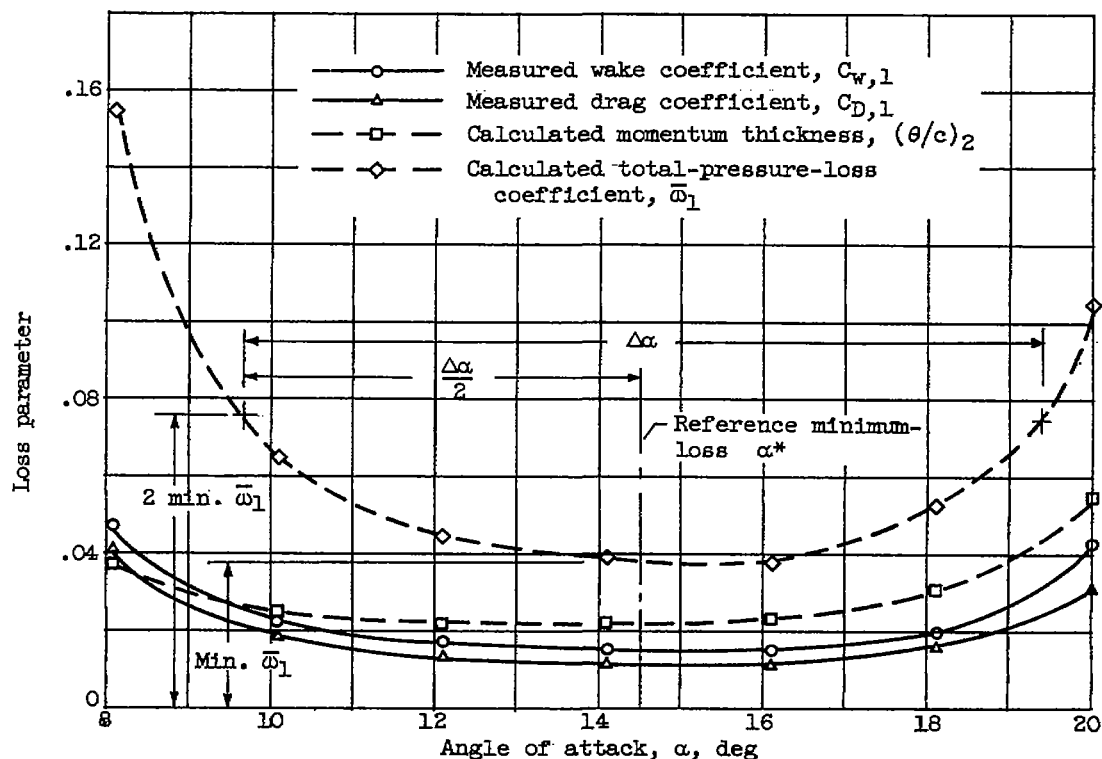


Figure 3. - Illustrative variation of measured and computed loss parameters and definition of reference minimum loss. Blade, NACA 65-(12A<sub>10</sub>)10; air inlet angle, 70°; solidity, 1.5 (ref. 9).

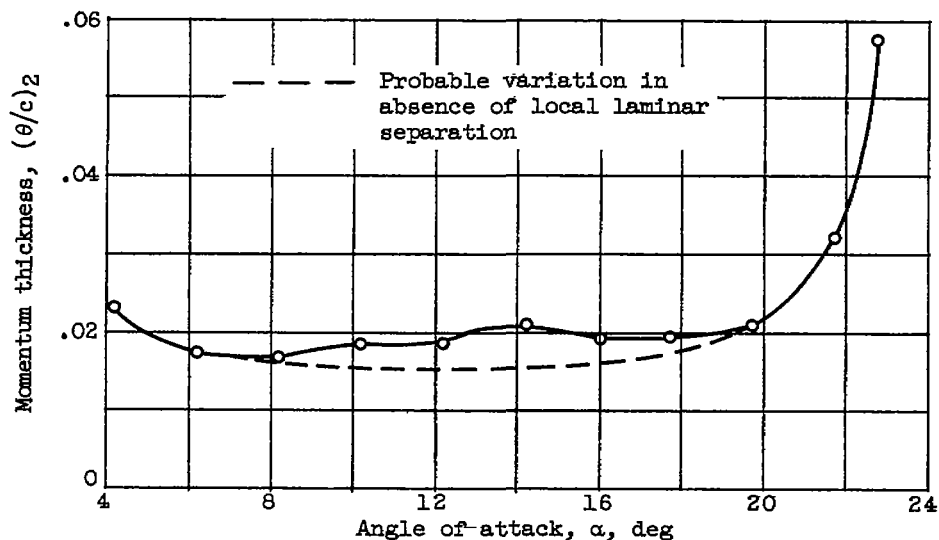
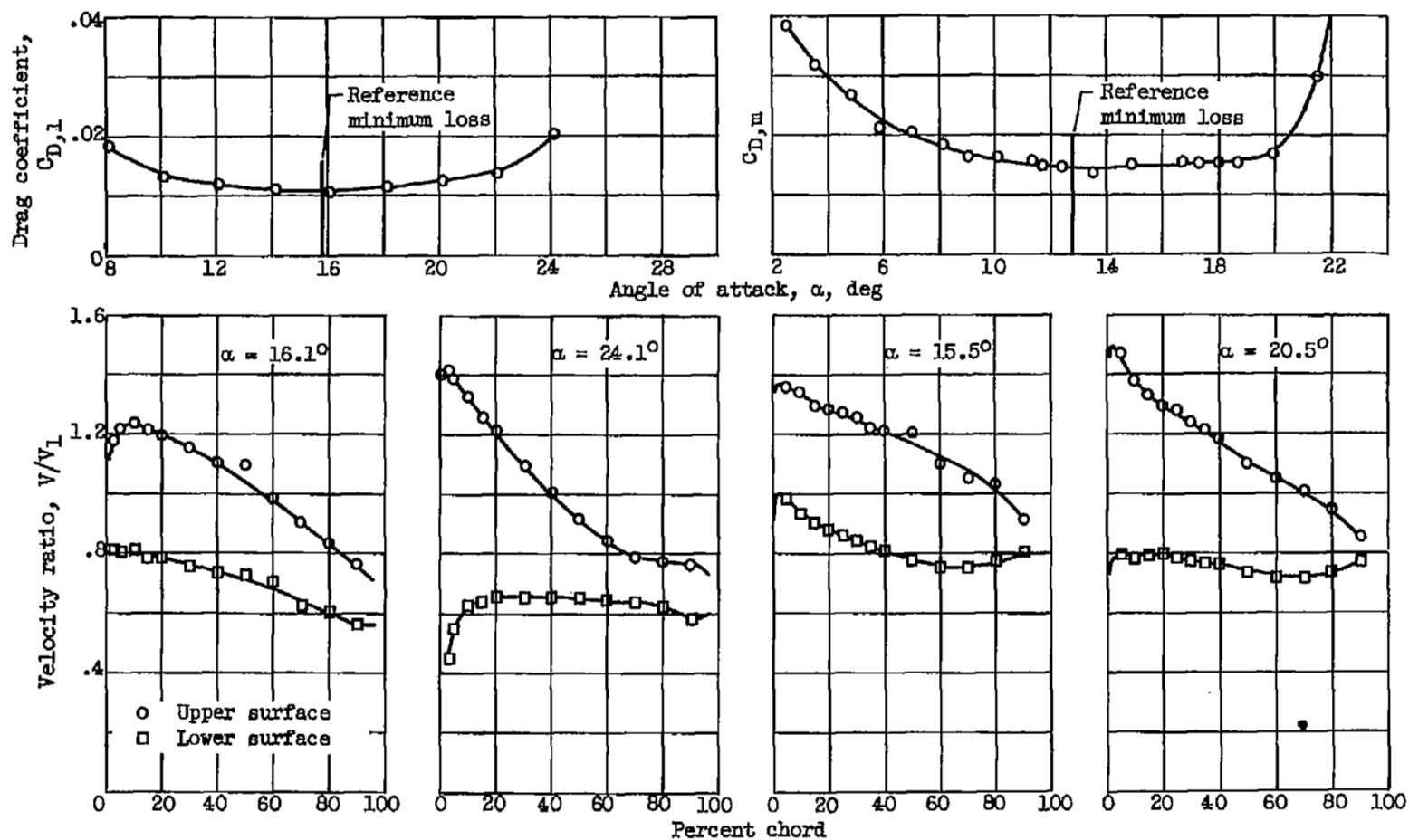


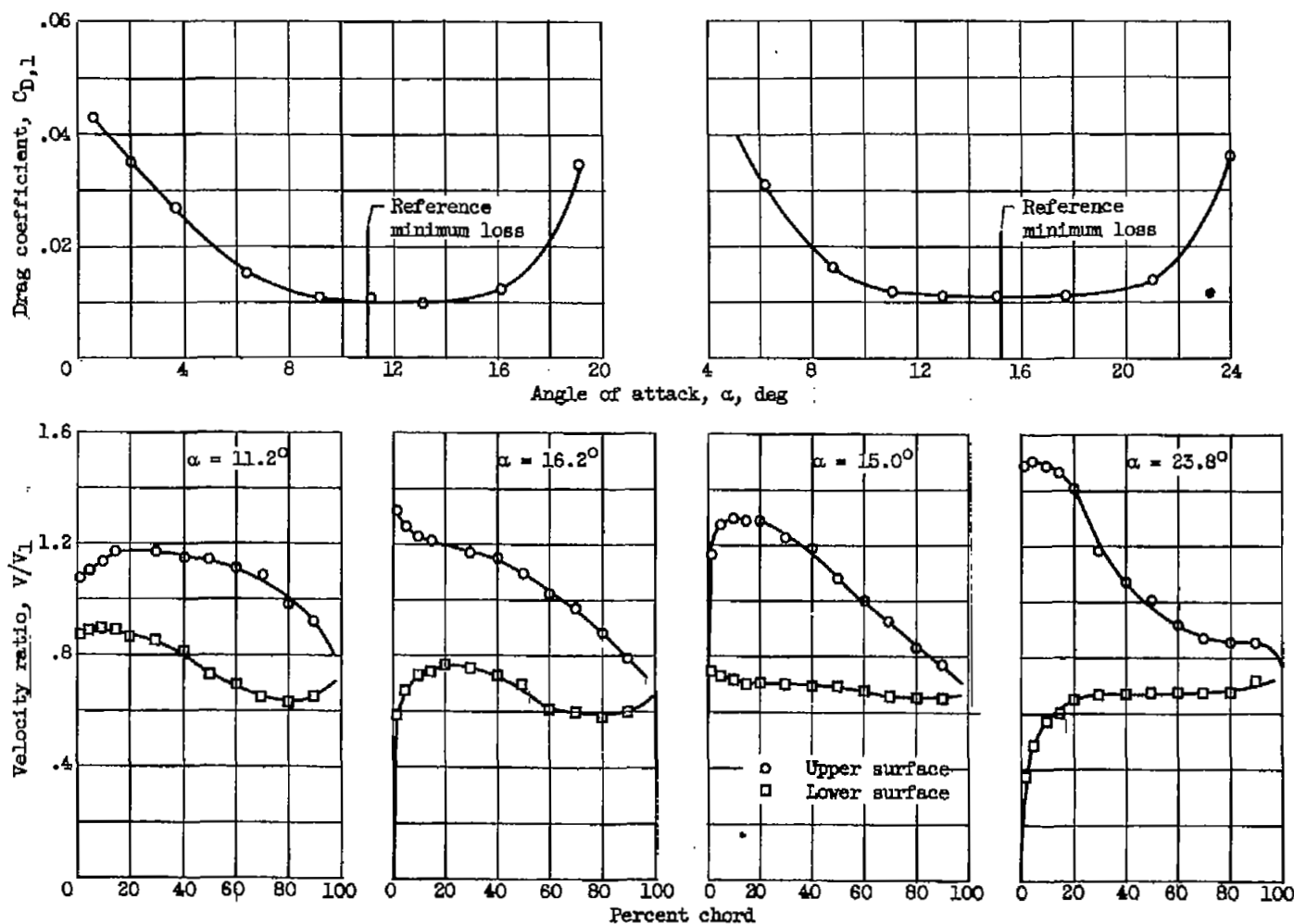
Figure 4. - Illustrative momentum-thickness variation in presence of local laminar separation. Blade, NACA 65-(12A<sub>10</sub>)10; air inlet angle, 60°; solidity, 1.0 (ref. 9).



(a) Blade, NACA 65-(12A<sub>10</sub>)10; air inlet angle,  $60^\circ$ ; solidity, 1.25 (ref. 9).

(b) Blade, British C.4 circular arc; blade-chord angle,  $29.5^\circ$ ; solidity, 1.0 (ref. 11).

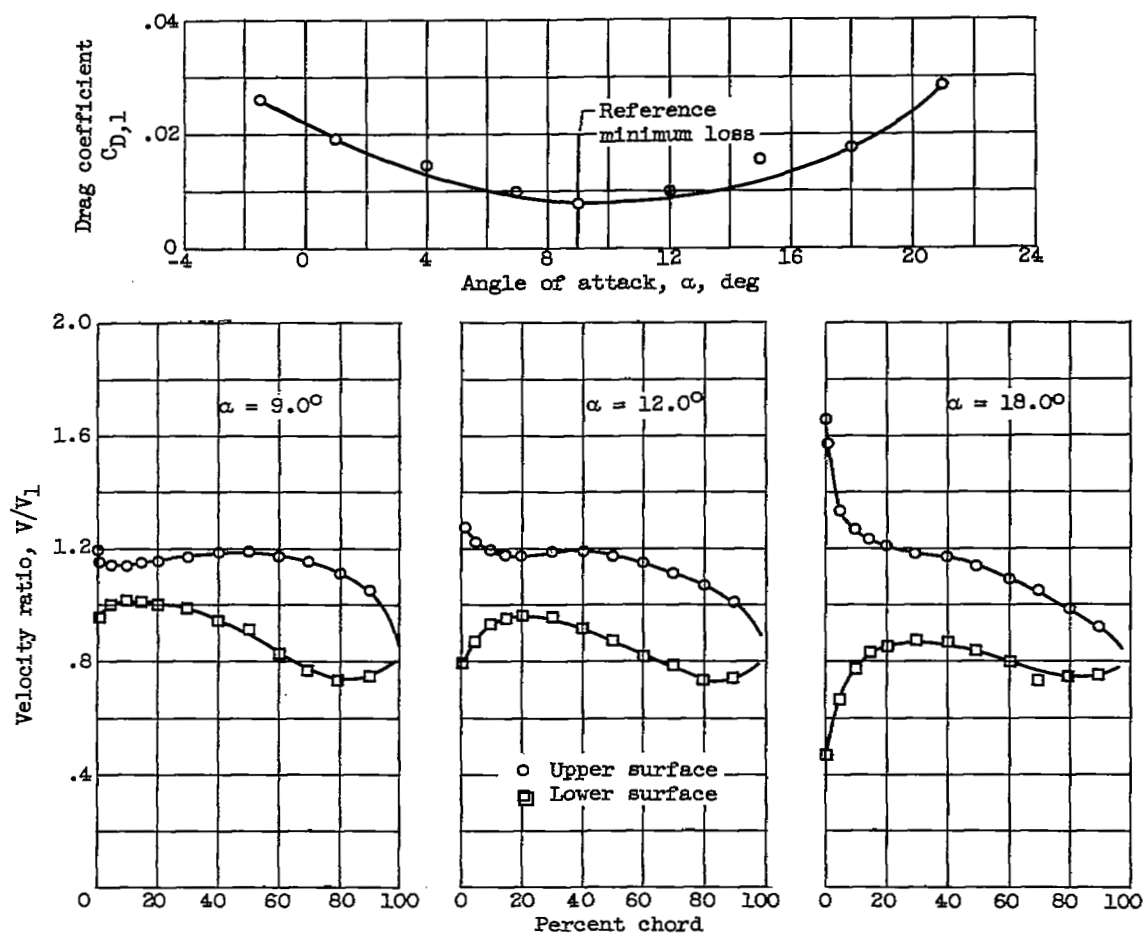
Figure 5. - Typical surface velocity distributions in region from minimum loss to positive stall for conventional cascade sections.



(c) Blade, NACA 65-(12A<sub>6</sub>I<sub>4b</sub>)10; air inlet angle,  $60^\circ$ ; solidity, 1.0 (ref. 10).

(d) Blade, NACA 65-(12A<sub>6</sub>I<sub>4</sub>)10; air inlet angle,  $60^\circ$ ; solidity, 1.0 (ref. 10).

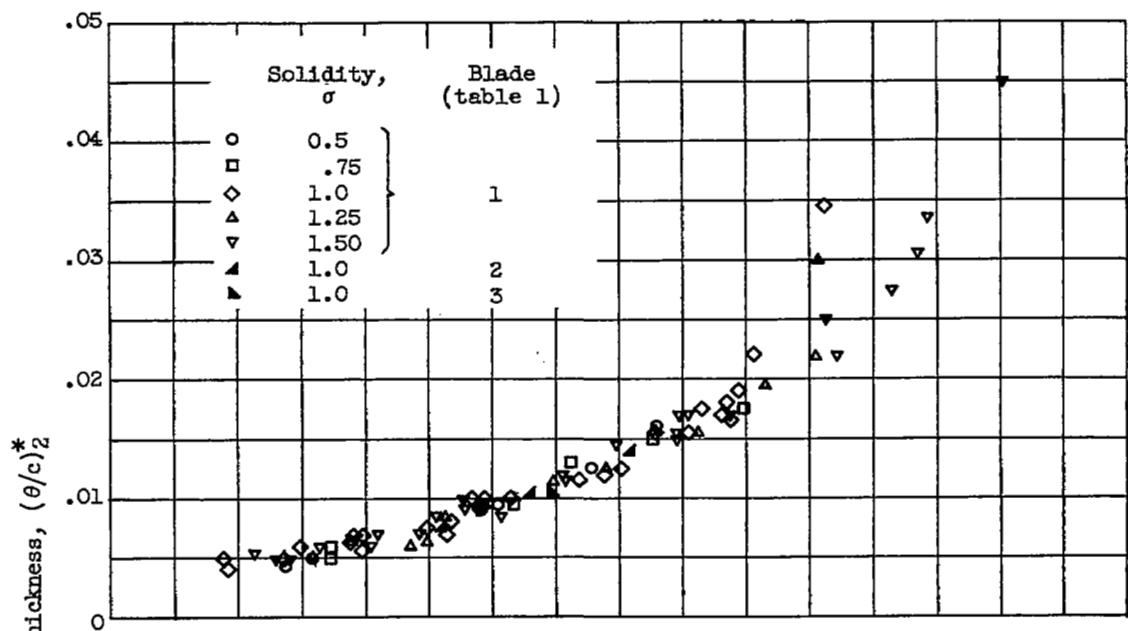
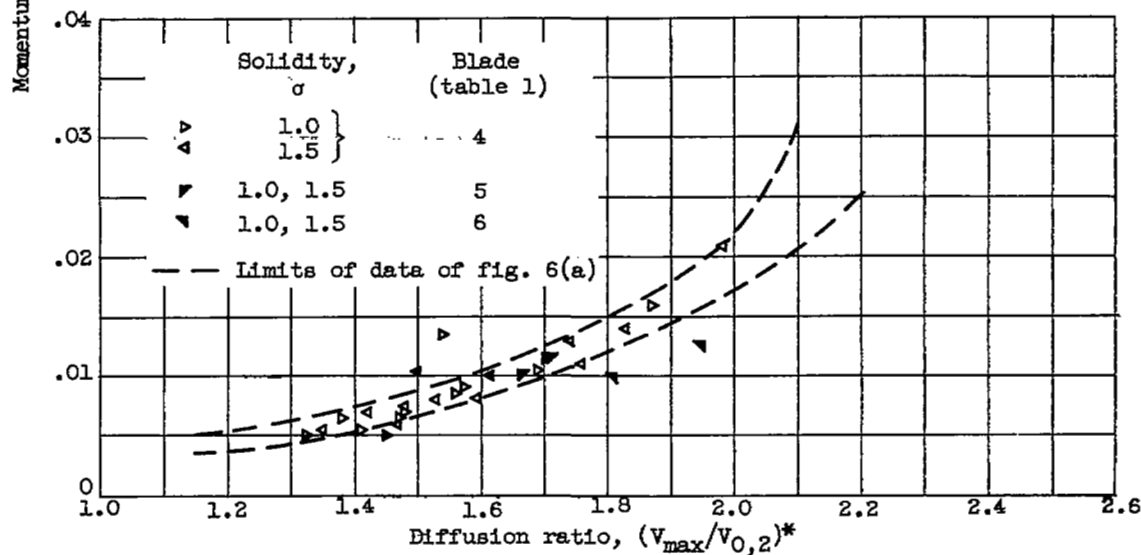
Figure 5. - Continued. Typical surface velocity distributions in region from minimum loss to positive stall for conventional cascade sections.



(e) Blade, NACA 65-(8A<sub>2</sub>I<sub>8b</sub>)10; air inlet angle, 45°; solidity, 1.0 (ref. 10).

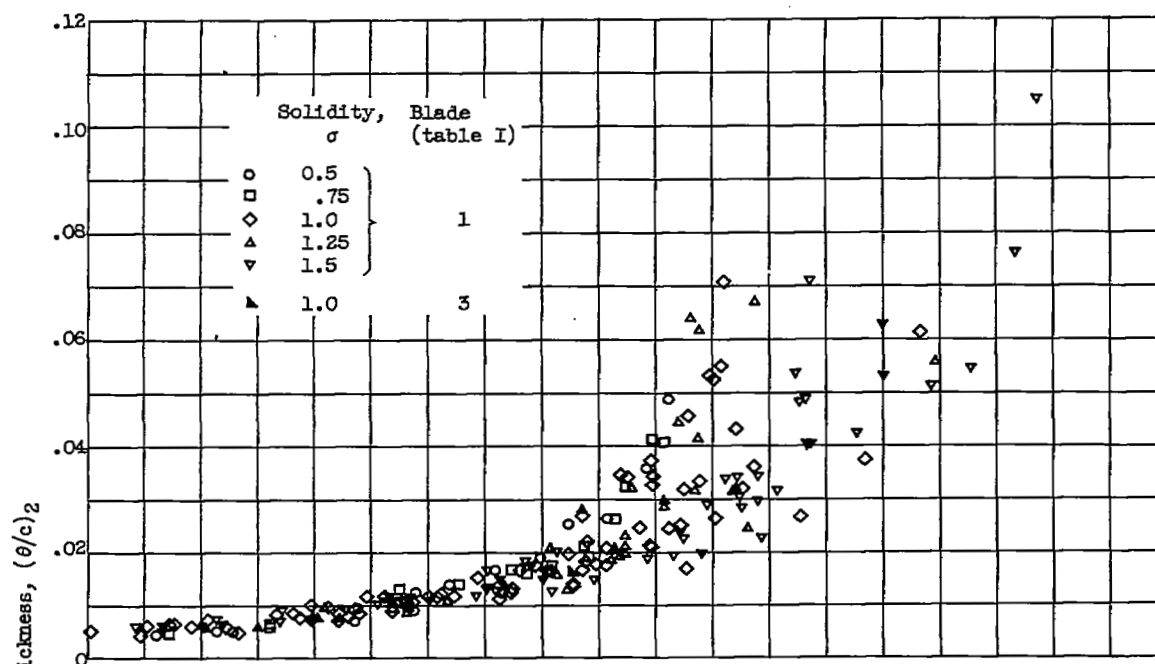
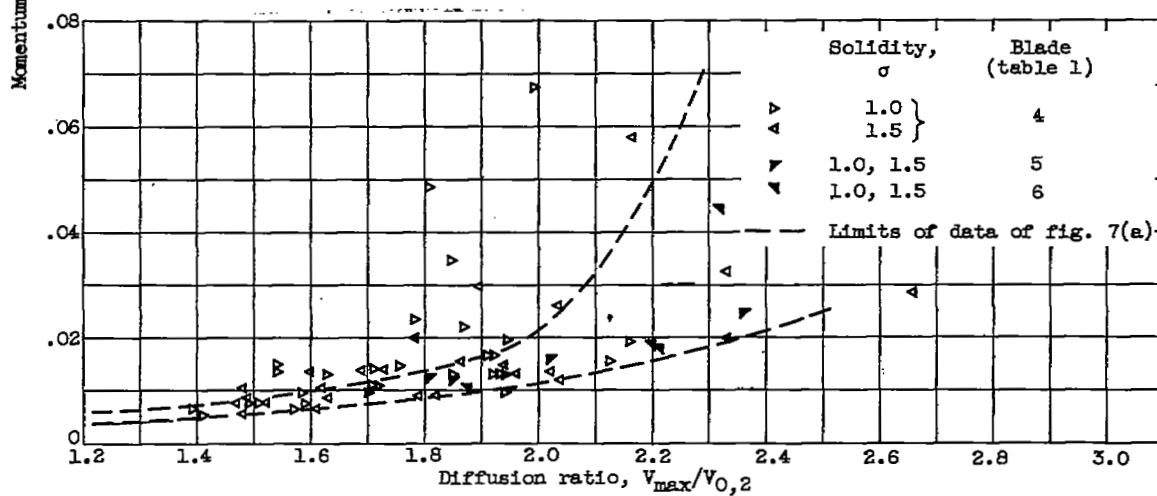
Figure 5. - Concluded. Typical surface velocity distributions in region from minimum loss to positive stall for conventional cascade sections.



(a) NACA 65-(A<sub>10</sub>)-Series and British C.4 circular-arc blades.

(b) NACA 65-(AI)-Series blades.

Figure 6. - Correlation of wake momentum thickness with upper-surface diffusion ratio at reference minimum-loss angle of attack.

(a) NACA 65-(A<sub>10</sub>)-Series and British C.4 circular-arc blades.

(b) NACA 65-(AI)-Series blades.

Figure 7. - Correlation of wake momentum thickness with upper-surface diffusion ratio at angles of attack greater than reference minimum loss.

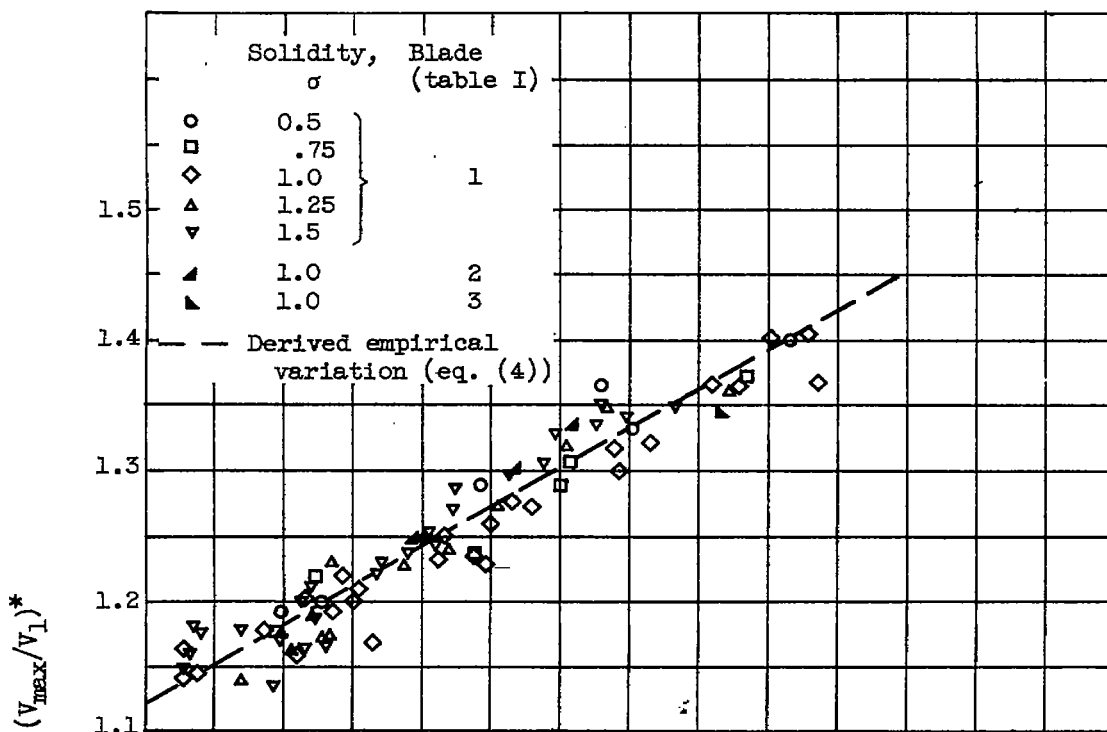
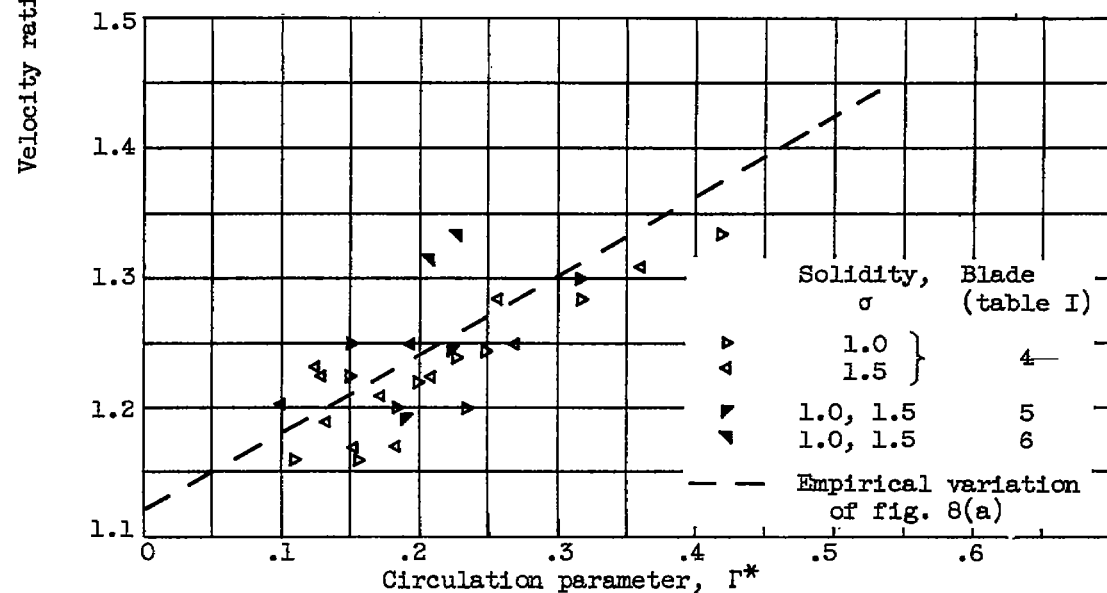
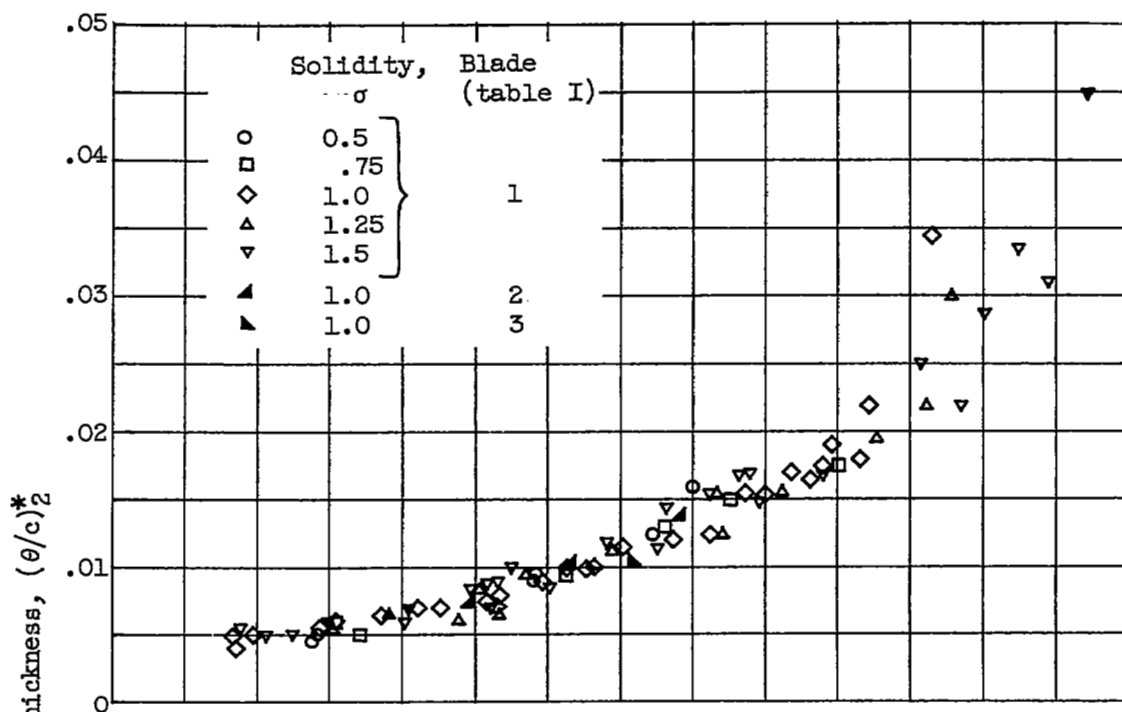
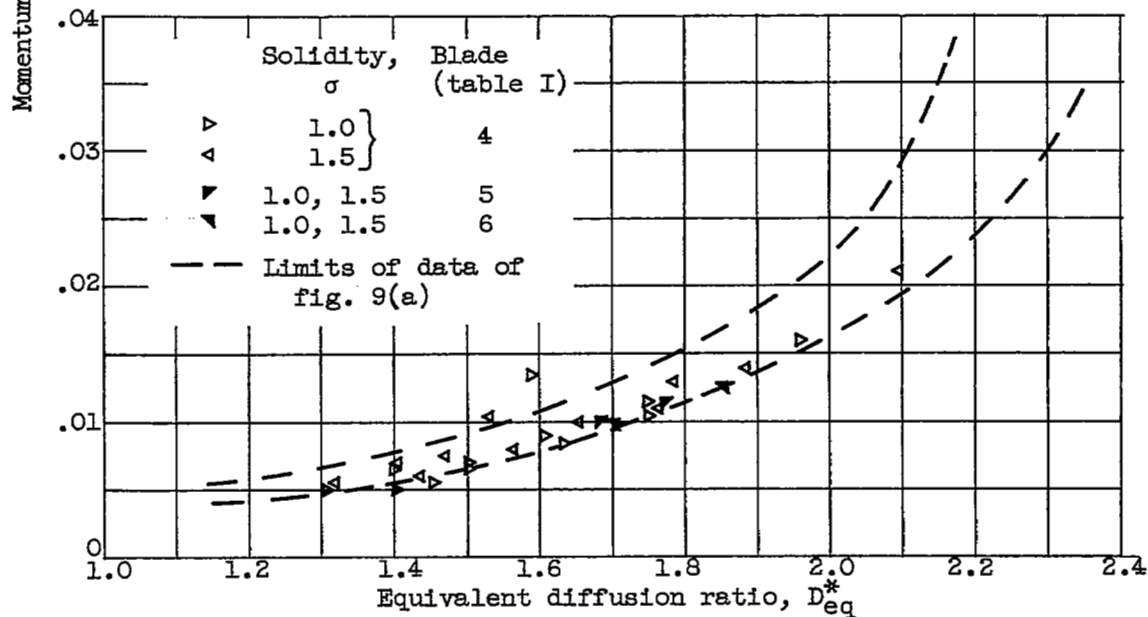
(a) NACA 65-(A<sub>10</sub>)-Series and British C.4 circular-arc blades.(b) NACA 65-(A<sub>I</sub>)-Series blades.

Figure 8. - Correlation of upper-surface velocity ratio with circulation parameter at reference minimum-loss angle of attack.

(a) NACA 65-(A<sub>10</sub>)-Series and British C.4 circular-arc blades.

(b) NACA 65-(AI)-Series blades.

Figure 9. - Correlation of wake momentum thickness with equivalent diffusion ratio at minimum-loss angle of attack.

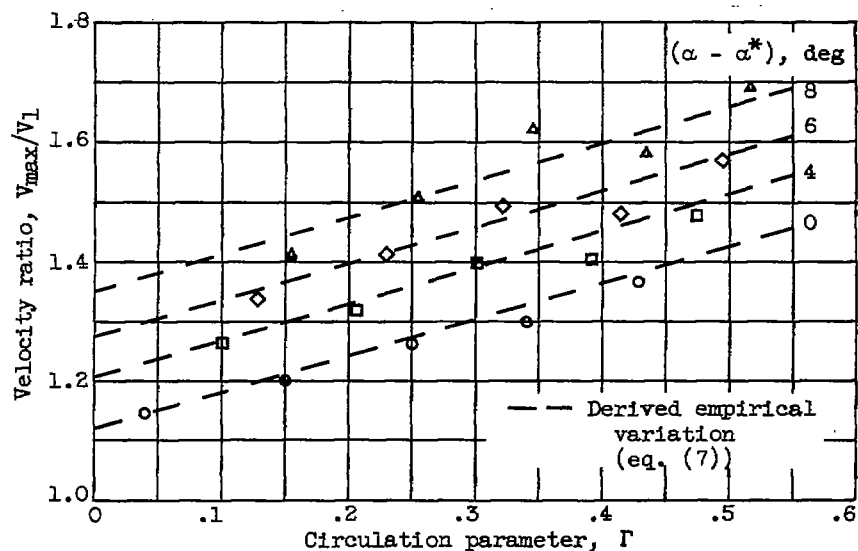


Figure 10. - Illustrative variation of correlation between upper-surface velocity ratio and circulation parameter for range of angle of attack. Blade, NACA 65-( $C_{l0}A_{10}$ )10; air inlet angle,  $30^\circ$ ; solidity, 1.0 (ref. 9).

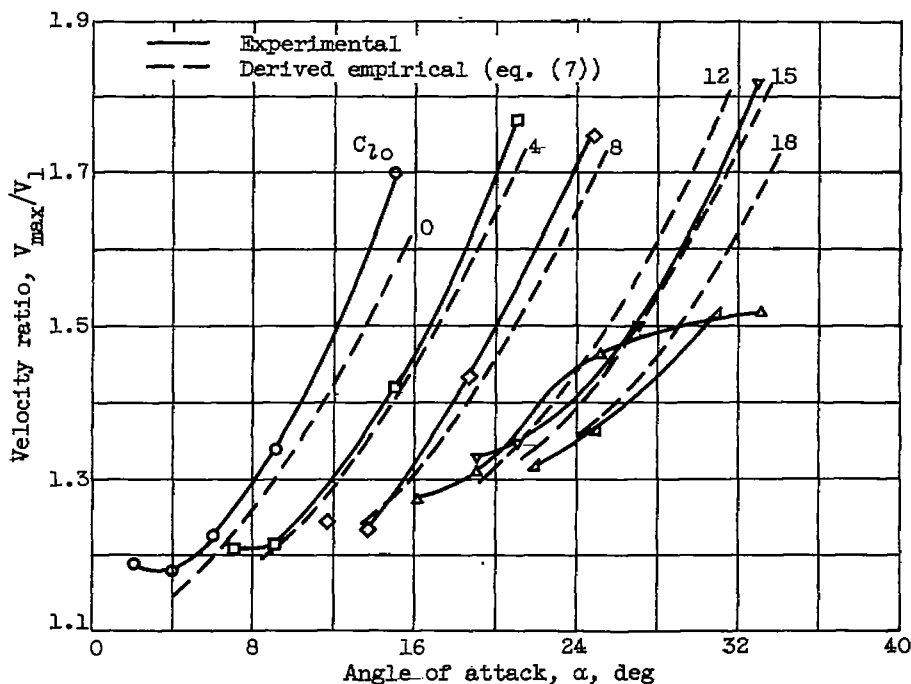


Figure 11. - Illustrative comparison of experimental and derived empirical variation of upper-surface velocity ratio. Blade, NACA 65-( $C_{l0}A_{10}$ )10; air inlet angle,  $30^\circ$ ; solidity, 1.5 (ref. 9).

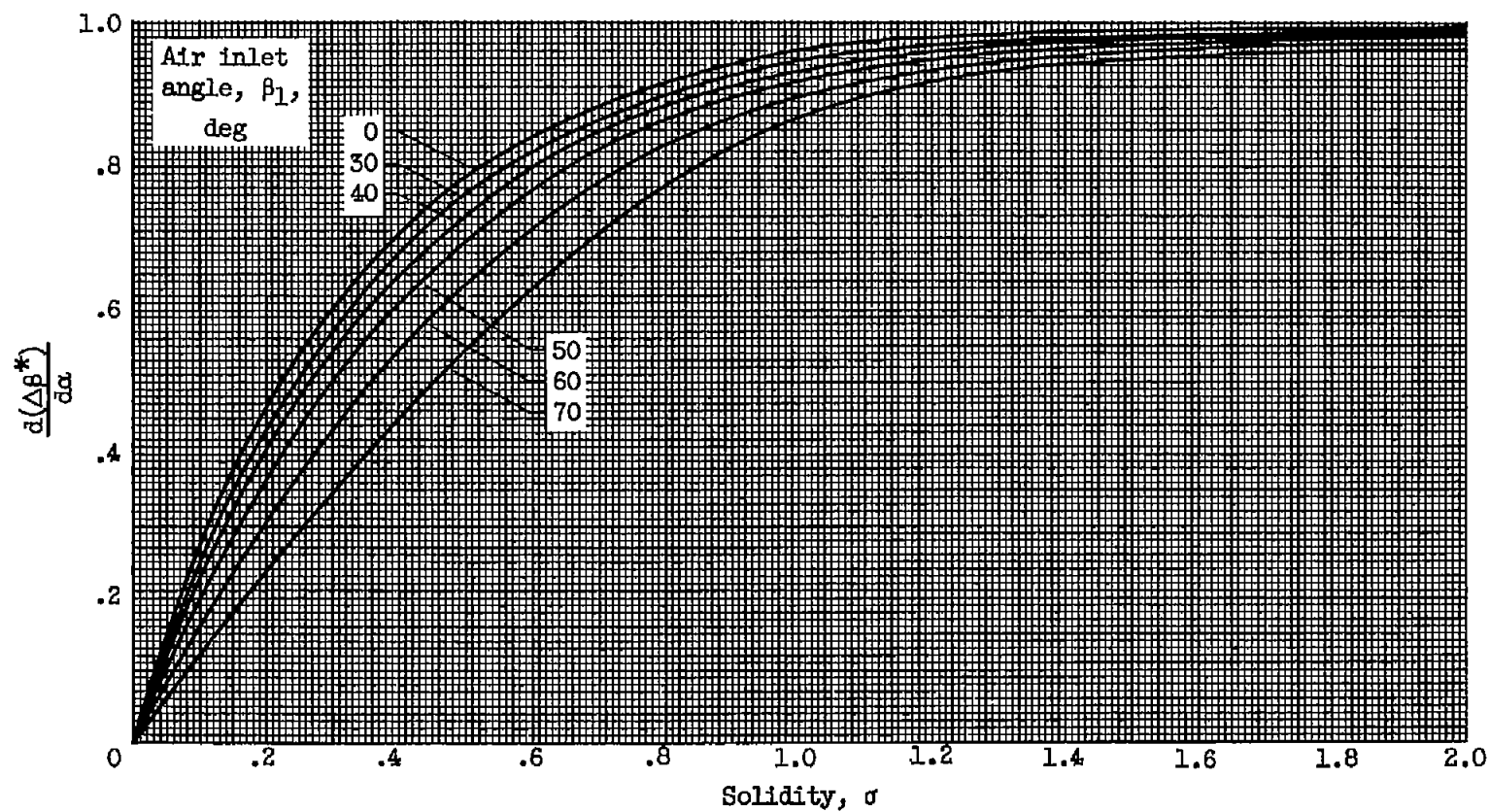
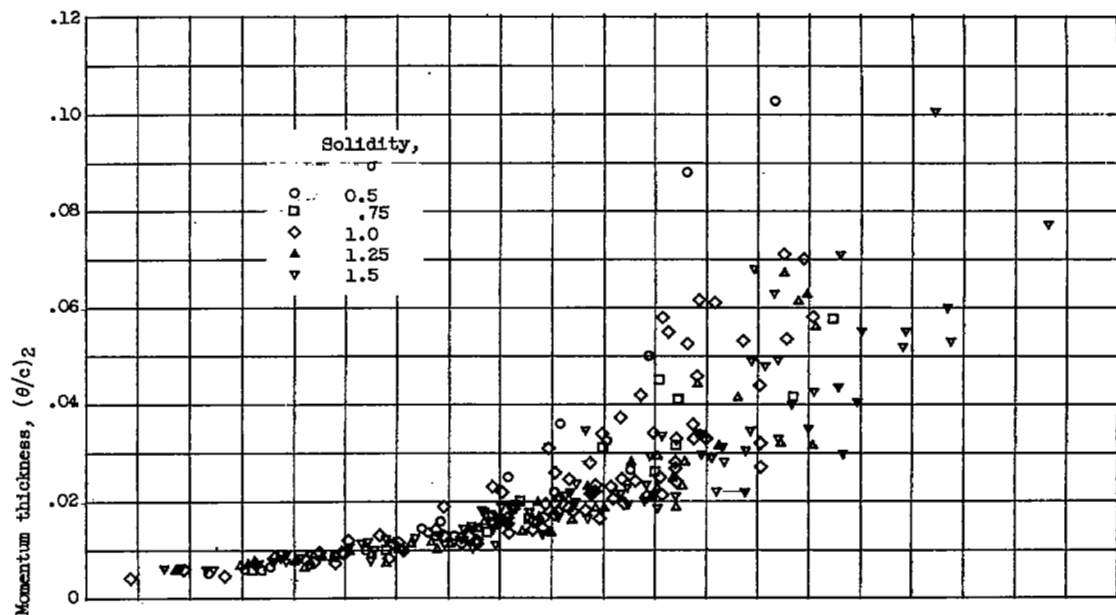
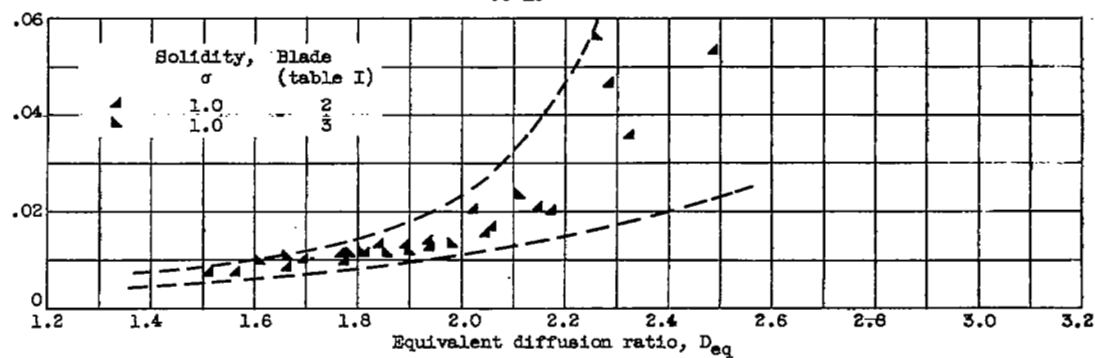


Figure 12. - Derived empirical variation of slope of turning angle against angle of attack at reference minimum-loss angle of attack.



(a) NACA 65-(C10A10)10 blades (blade 1).



(b) British C.4 circular-arc blades.

Figure 13. - Correlation of wake momentum thickness with equivalent diffusion ratio at angles of attack greater than minimum loss.

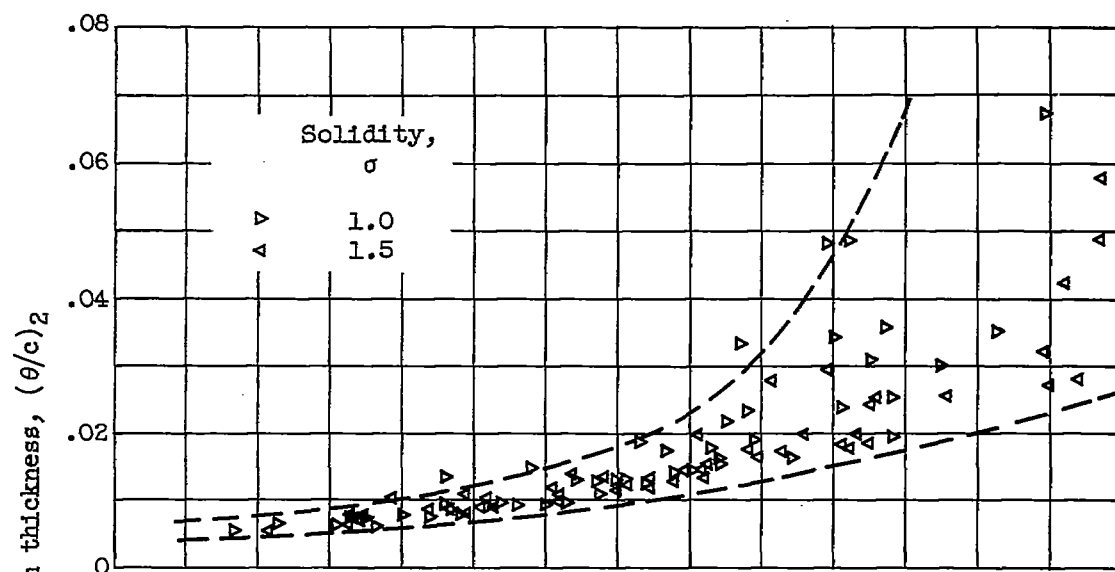
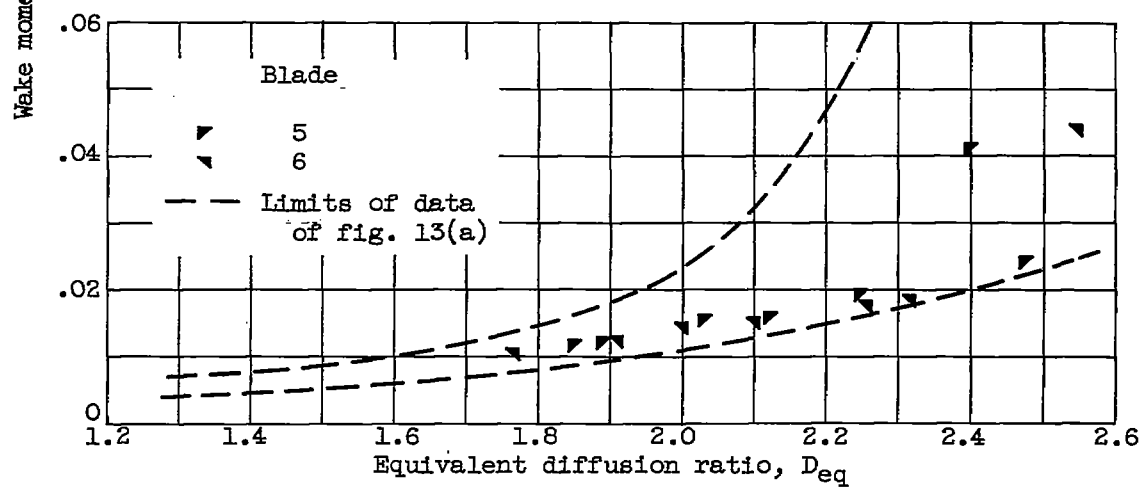
(c) NACA 65-(C<sub>7</sub>O A<sub>2</sub> I<sub>8b</sub>)10 blades (blade 4).(d) NACA 65-(12A<sub>6</sub> I<sub>4</sub>)10 and 65-(12A<sub>6</sub> I<sub>4b</sub>)10 blades.

Figure 13. - Concluded. Correlation of wake momentum thickness with equivalent diffusion ratio at angles of attack greater than minimum loss.



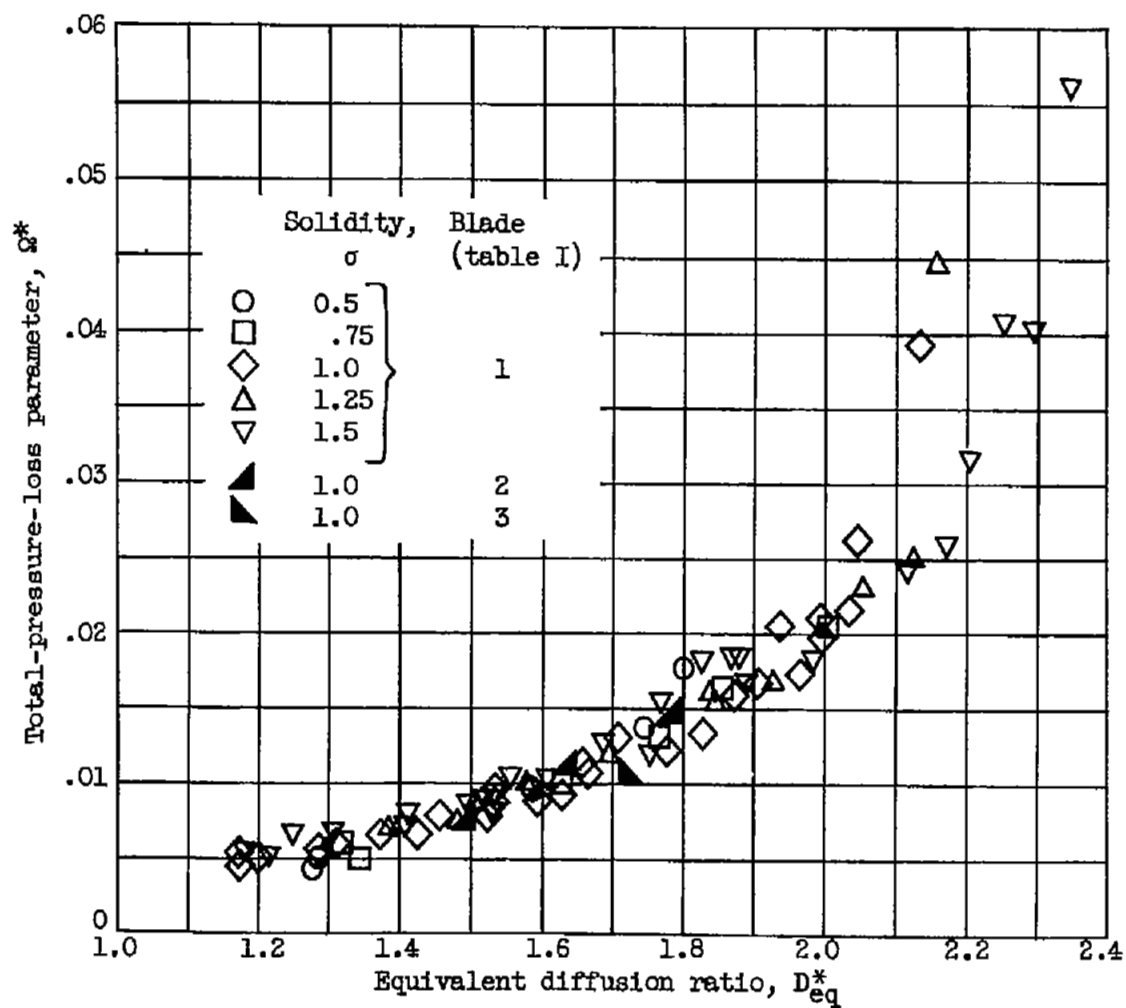


Figure 14. - Correlation of total-pressure-loss parameter with equivalent diffusion ratio at minimum-loss angle of attack.

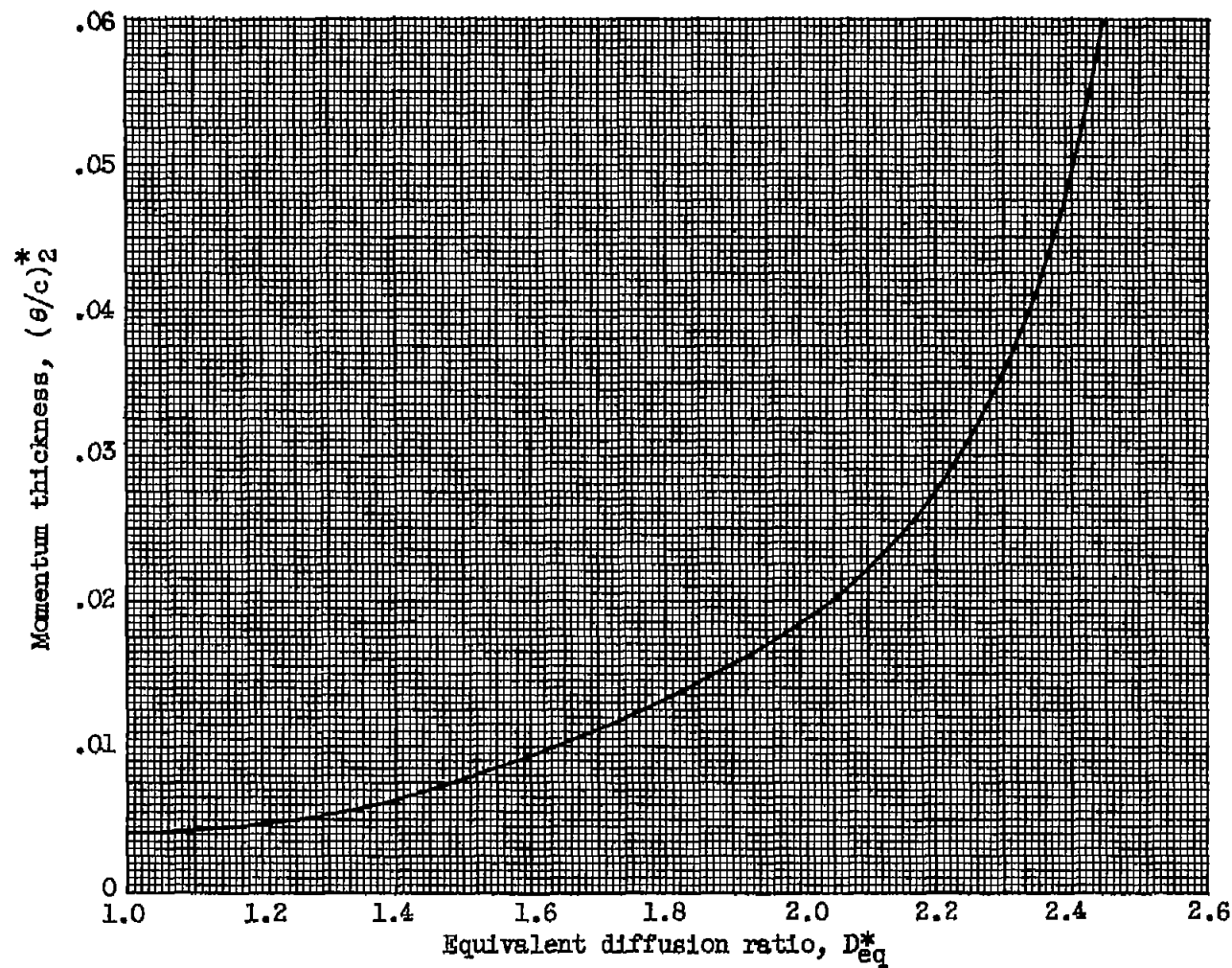


Figure 15. - Representative variation of wake momentum thickness with equivalent diffusion ratio at minimum-loss angle of attack used in calculations of cascade loss variations.

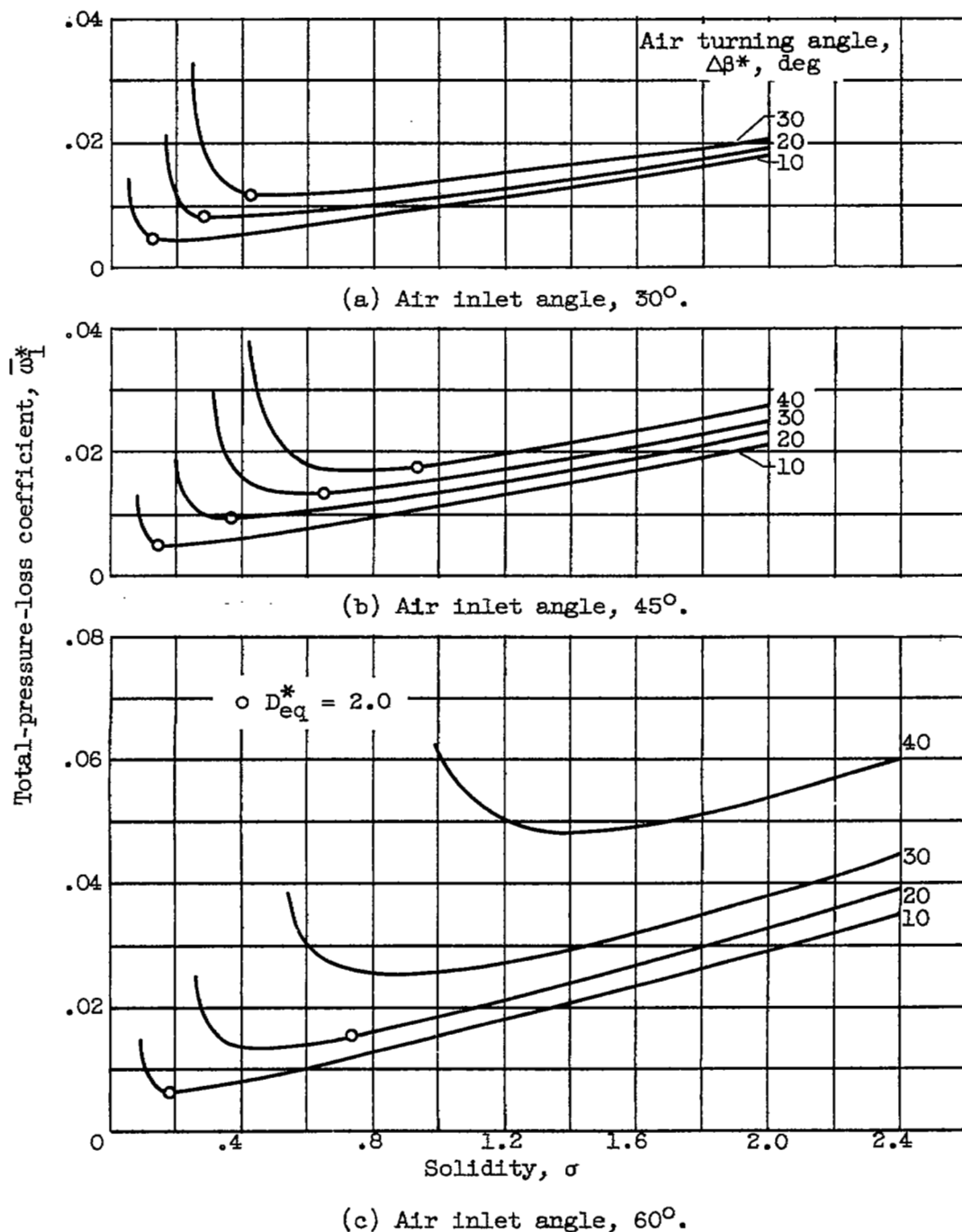


Figure 16. - Calculated variation with solidity of low-speed total-pressure-loss coefficient at minimum-loss angle of attack for conventional compressor cascade blades. Maximum-thickness ratio, 0.10.

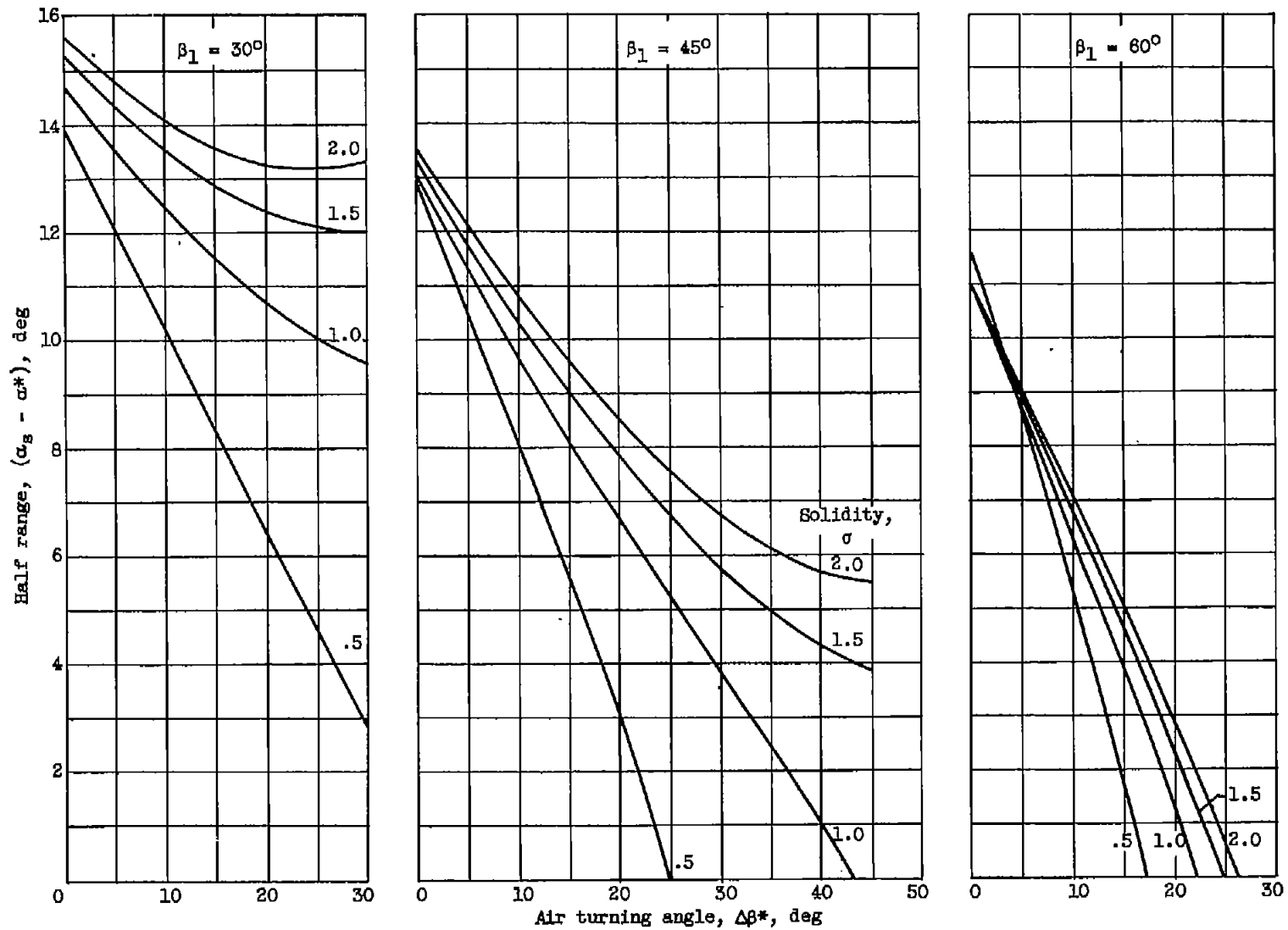


Figure 17. - Calculated variation with minimum-loss air turning angle of low-speed half range from minimum loss to positive stall. (Stall at  $D_{eq} = 2.0$ ; fixed air inlet angle.)

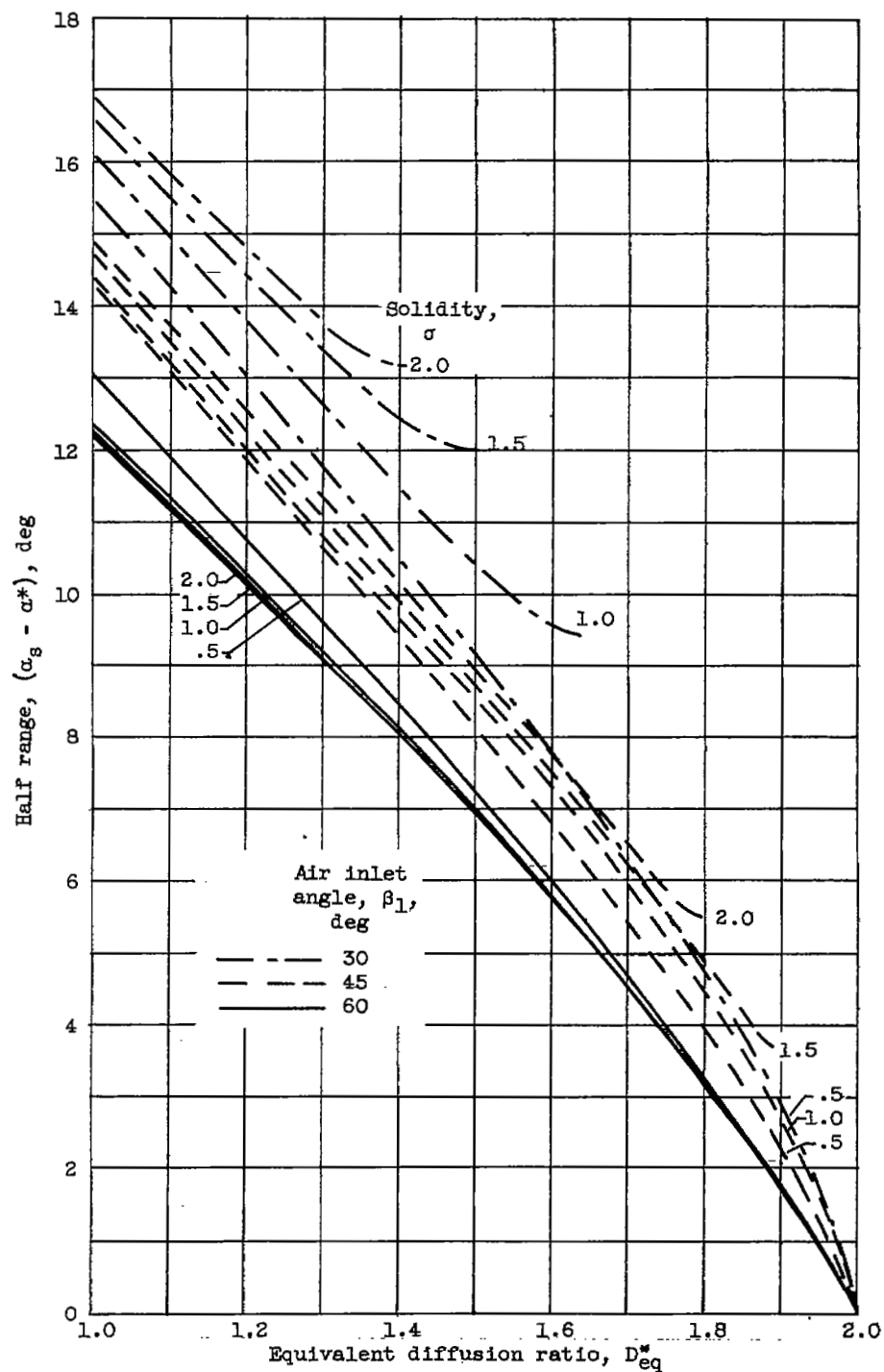


Figure 18. - Calculated variation of half range from minimum loss to positive stall with equivalent diffusion ratio at minimum loss. (Stall at  $D_{eq} = 2.0$ ; fixed air inlet angle.)

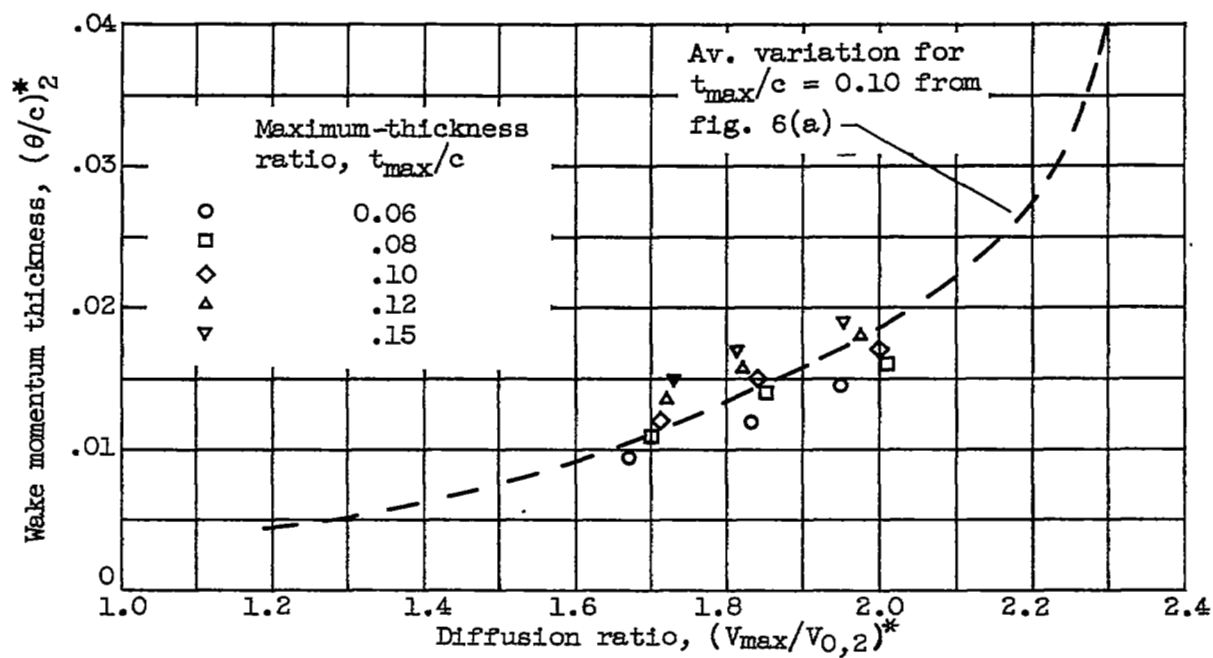


Figure 19. - Variation of wake momentum thickness with upper-surface diffusion ratio at minimum loss for 65-(12A<sub>10</sub>)10 blade with varying maximum-thickness ratio (data from ref. 16).

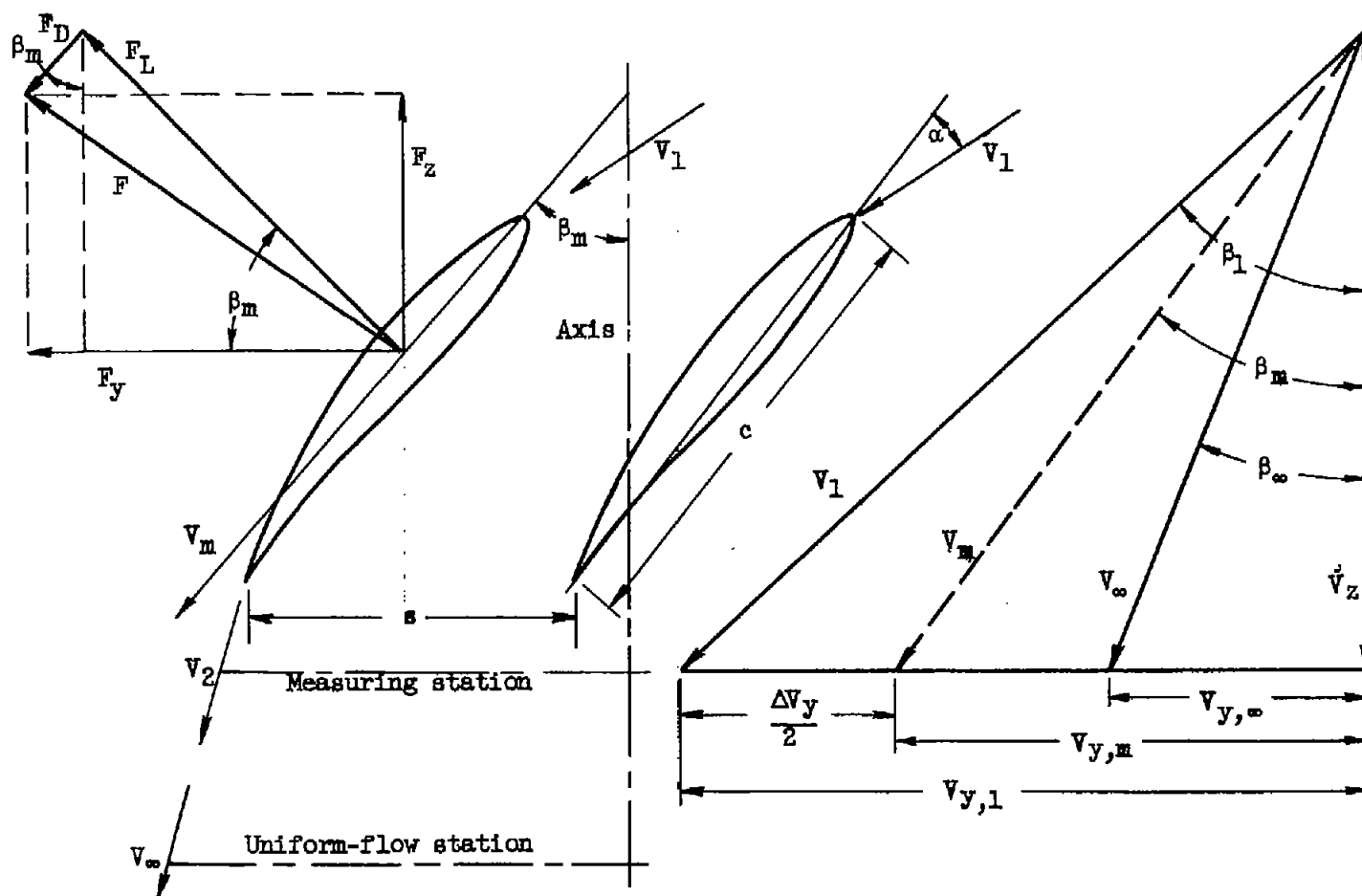


Figure 20. - Force and velocity diagrams for blade in two-dimensional incompressible cascade flow.

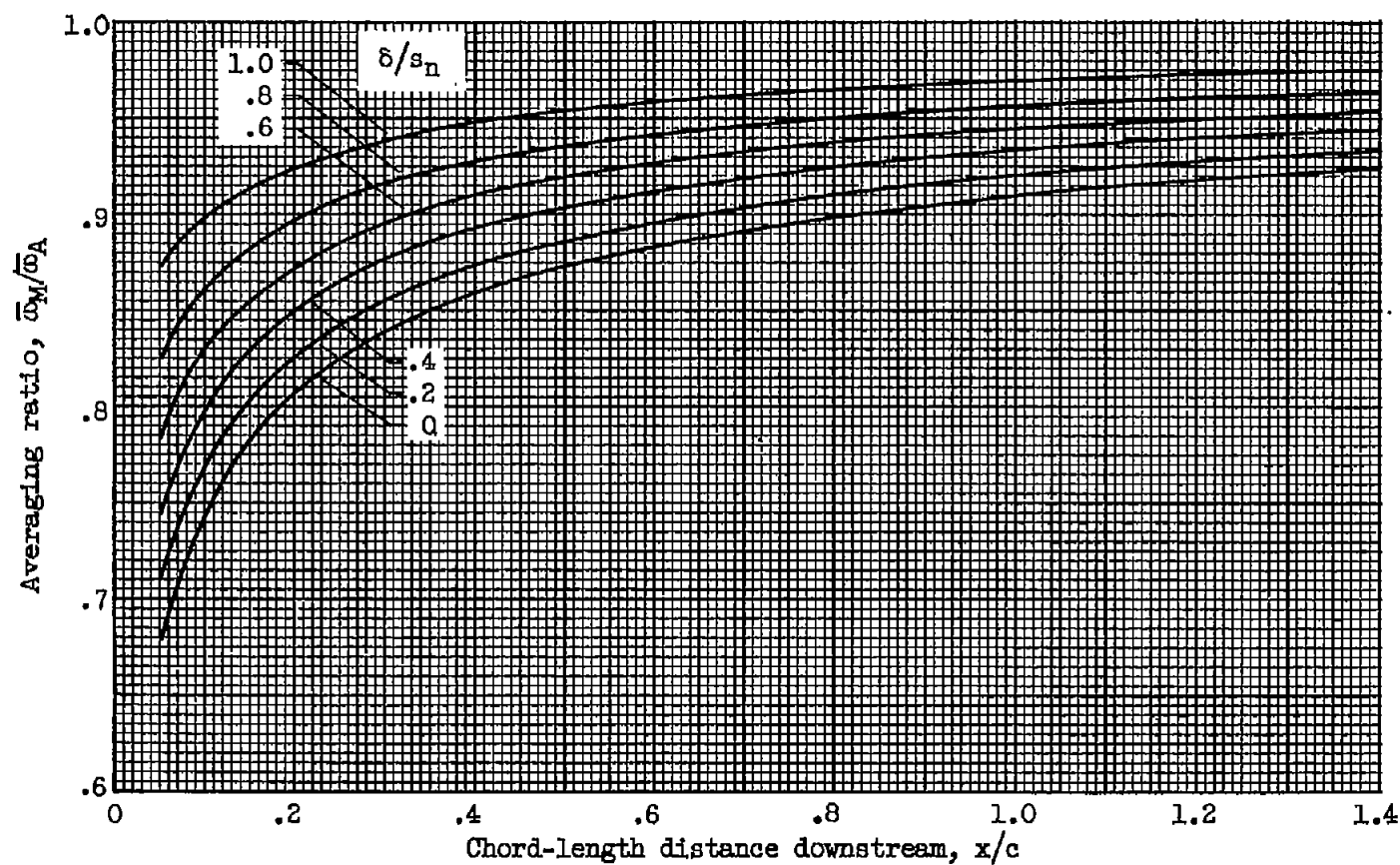


Figure 21. - Derived downstream variation of ratio of mass-averaged to area-averaged loss in total pressure in blade wake from reference 2.



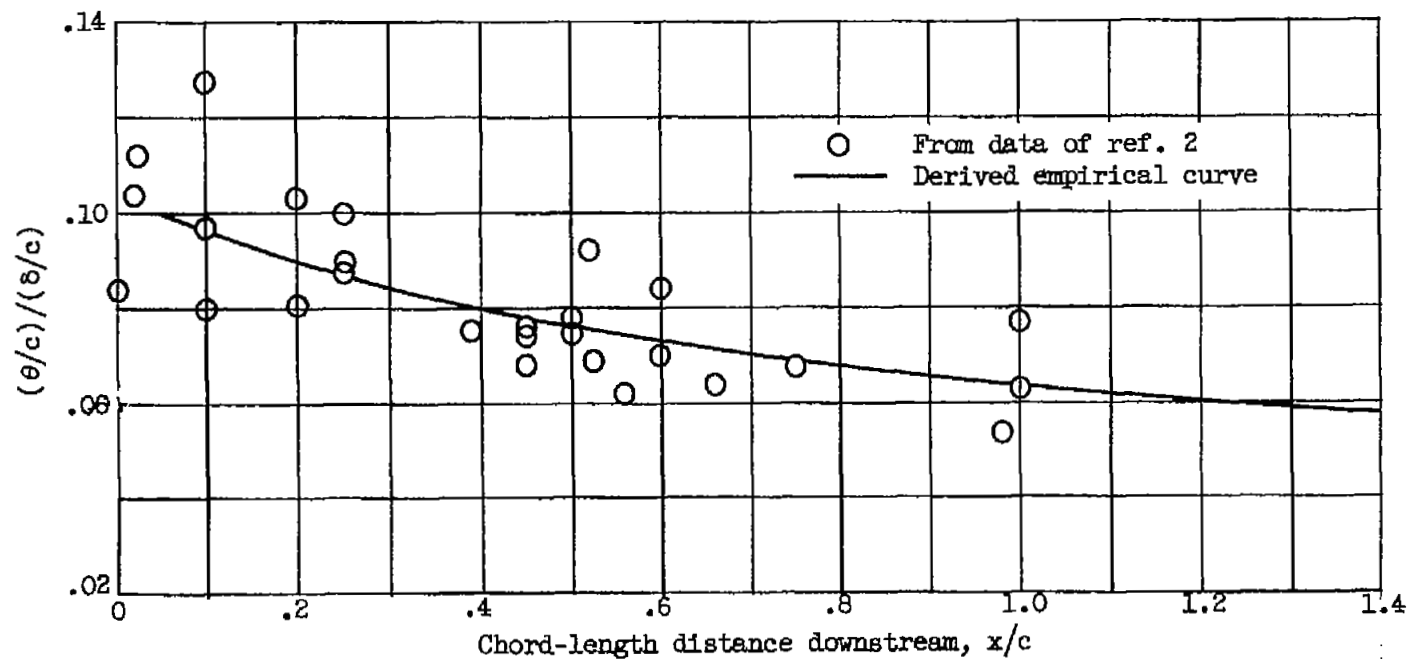



Figure 22. - Downstream variation of ratio of wake momentum thickness to wake full thickness.

[REDACTED]

LANGLEY RESEARCH CENTER



3 1176 01331 0165

[REDACTED]

[REDACTED]

11

11

[REDACTED]